April 2013

Analysis of the thermo-mechanical reliability of an SMT attachment

Congji Li
Worcester Polytechnic Institute

Michael Charles Bartlett
Worcester Polytechnic Institute

Richard Alex Beski
Worcester Polytechnic Institute

Roberto Antonio Alvarado
Worcester Polytechnic Institute

Santiago Isaza
Worcester Polytechnic Institute

Analysis of the thermo-mechanical reliability of an SMT attachment

By

Roberto Alvarado
Michael Bartlett
Richard Beski
Santiago Isaza
Congji Li

NEST- NanoEngineering, Science, and Technology
CHSLT- Center for Holographic Studies and Laser Micro-MechaTronics
Mechanical Engineering Department
Worcester Polytechnic Institute
Worcester, MA 01609-2280

25 April 2013

1. Acknowledgements

We would like to thank Professor Ryszard Pryputniewicz for his effort and hard work in advising and making this project possible. We would also like to thank Dr. Adriana Hera, and Peter Hefti for their assistance and support in providing resources in aid of our project. We would like to thank Yu Xiao for providing us with boards to analyze, as well as test. Lastly we would like to thank Jeff Koebrich and Watchfire Signs for providing an insight into SMTs and their usage in the manufacturing sector.

2. MQP proposal summary

Microsystems, microelectronics, and MEMS are all new technologies that are being increasingly integrated into society and everyday life. The face of microtechnology is constantly changing as both hardware and software join hands to push the limits of imagination to meet the ever-growing needs of the public. As society becomes more heavily dependent on electronics and the microtechnology behind them, it has become increasingly important to test and analyze the reliability of the products. Some of the main concerns in the reliability of microelectronics are the solders, leads and packages within the systems. Our major qualifying project (MQP) aimed to develop a process that would allow us to observe, test, and analyze the different types of failures that occur in microelectronics that make use of surface mount technology. We had intended to begin with extensive literary research on the history of the technology and how it has advanced in the past, what types of failures and issues commonly occur, how any failures and issues are currently being addressed, and what type of research has already been conducted on the subject. We planned to contact manufacturers and industry leaders that utilize SMT in their products to understand the current state of these issues, in order to gain a perspective of how prevalent the failures of SMT systems are and how they are being mitigated. We also intended to obtain an idea of what these industry leaders see in the future of SMT, so that our conclusions and results could be geared towards the future. Lastly we developed and conducted our own preliminary research on SMT using both lab techniques that measure stresses and strains and finite element analysis software where we can simulate stresses and strains. We would then be able to closely observe the failures of components and develop our own conclusions to compare to those of industry leaders. To understand what causes these failures we looked into areas such

as the design parameters of the joints as well as the fatigue properties of the solder. After all the data had been collected and analyzed we expected to determine failures that currently occur in SMT components, what the root causes of these failures are and what methods may be used to correct the issues. Through identification and analysis, we aimed to decrease the severity of these failures while increasing the overall reliability of SMTs. We envisioned that these results would prove to be very useful to industry leaders that make use of SMTs.

Keywords: SMT, thermo-mechanical, deformation, reliability, FEA, solder, joint, attachment, stress, strain, fatigue, vibration, thermal expansion mismatch, uncertainty analysis

3. Objective

The objective of this MQP was to analyze the reliability of SMT attachments that are subjected to electrical, thermal, and mechanical loads. Since microsystems, microelectronics, and micro-electro-mechanical systems (MEMS) are being increasingly integrated into society and everyday life, reliability is of major concern. Of the many factors contributing to SMT reliability, this project aims to identify the most prevalent issue through modeling and uncertainty analysis.

4. Abstract

Microsystems, microelectronics, and MEMS are all new technologies that are being increasingly integrated into society and everyday life. These technologies are constantly changing as both hardware and software are integrated to push the limits of imagination to meet the ever-growing needs of the consumer. Some of the main concerns in the reliability of micro-electronics are the solders, leads and packages within the systems. Our MQP involved the observation, testing, and analysis of the different types of failures that occur in surface mount technology (SMT). We have conducted extensive literary research on the history of the technology and how it has advanced in the past, what failures and issues commonly occur, how failures and issues are being addressed, and what research has already been conducted on the subject. We have contacted manufacturers and industry leaders that utilize SMT to understand the current state of these issues, in order to gain a perspective of how prevalent the failures of SMT systems are and how they are being mitigated. Lastly, we used finite element analysis (FEA) software to test failures due to, but not limited to, vibrations, thermal expansion mismatch, and material properties. We correlated the results of our modeling with laboratory testing and supportive detailed uncertainty analysis.

Keywords: SMT, thermo-mechanical, deformation, reliability, FEA, solder, joint, attachment, stress, strain, fatigue, vibration, thermal expansion mismatch, uncertainty analysis

5. Nomenclature

°C	Degrees Celsius
ANSYS	Computational analysis software (ANSYS Workbench)
C	Non-ideality coefficient
CAD	Computer aided design
COMSOL	Computational analysis software (COMSOL Multi-physics)
CQFP	Ceramic quad flat pack
CSV	Comma separated value
Cu	Copper
Cu-Sn	Copper-tin alloy
d	Fatigue ductility coefficient
e	Fatigue ductility exponent
ES	Young modulus of solder
FEA	Finite element analysis
FS	Factor of safety
H	Height
HCF	High cycle fatigue
IEEE	Institute of Electrical and Electronics Engineers, Incorporated
IMC	Intermetallic compound
K	Kelvin
LCC	Leadless chip carrier
LED	Light emitting diode
L_o	Characteristic length
MEMS	Micro-electro-mechanical Systems
MPa	Mega-Pascals (Unit of pressure)
MQP	Major Qualifying Project (Undergraduate thesis)
N_f	Number of cycles to failure
PCB	Printed circuit board
SMD	Surface mount device
SMT	Surface mount technology
SOJ	Small outline J-lead package
SolidWorks	CAD software
Sn-Pb	Tin-lead alloy
T_{amb}	Ambient temperature
Tcc	Chip carrier temperature
THT	Through-hole technology
T_o	Ambient temperature
T_{PCB}	Printed circuit board/substrate temperature

T_s	Substrate/printed circuit board temperature
T_{sm}	Mean solder temperature
V	Volts
W	Watts
WPI	Worcester Polytechnic Institute
α_{cc}	Chip carrier coefficient of thermal expansion
α_{PCB}	Printed circuit board/substrate coefficient of thermal expansion
α_S	Solder coefficient of thermal expansion
δNf	Uncertainty in the number of cycles to failure
$\delta Nf\delta d$	Fatigue ductility coefficient contribution to uncertainty in number of cycles to failure
$\delta Nf\delta e$	Fatigue ductility exponent contribution to uncertainty in number of cycles to failure
$\delta Nf\delta\gamma$	Shear strain contribution to uncertainty in number of cycles to failure
γ_c	Shear strain
ε_{TS}	Thermal strain in solder
σ_{TS}	Thermal stress in solder
σ_{yS}	Yield strength of solder
τ_c	Thermal expansion mismatch

6. Table of contents

7. List of figures

8. List of tables

9. Literature review

9.1. What is SMT?

A surface mounted technology (SMT) is defined as a methodology for attaching packages to one side of a printed circuit board (PCB) by way of a solder joint. These solder joints attach the leads of a package to the PCB right on the surface. Prior to the implementation of SMT, the type of attachments used comprised of one main type: through-hole technology (THT). As the name suggests, THT connects to the boards by pins penetrating the board that are secured with solder on both sides. For ease of distinction, our group has associated leads with SMTs and pins with THTs. As a result of the pierced boards attachments could only be placed on one side since the electrical connections are only usable on the side of the board with the attachment. SMTs have the advantage over THTs in this way, as SMTs don't perforate the boards, allowing for electrical connections on both sides of the board and in turn attachments on both sides.

The use of leads with SMT is more preferable than the use of pins found in THT. Leads generally require less space on a board than pins do, as the connections only need one side of the board to be effective. SMTs are thus able to occupy less space on a board than THTs. With this smaller size the potential to have more packages/components located on one PCB becomes present. Attachment size plays a pivotal role in how effective and reliable the attachment can be. Larger attachments have the capability to succumb to some types of failures easier than smaller attachments. These failures can be represented in the realms of vibration, thermal cycling, as well as other loads the packages may be exposed to. Due to the size of attachments, SMTs fall into the category of a smaller attachment than most THTs, providing the potential for more

SMTs to be used on a PCB compared to the number of possible THTs. With this all considered SMTs are more versatile and resistant to failures compared to THTs, making SMTs more effective and more reliable attachments.

9.2. What are the issues to explore?

9.2.1. Piezoresistivity

An effect called piezoresistivity affects both SMTs and surface mount devices (SMDs) alike (Kühl 1999). Piezoresistivity is a phenomenon that simply alters the resistance of a select SMT or SMD upon being subject to bending. Piezoresistivity occurs, even upon minimal bending of a PCB, on the order of a few millimeters (0-5mm) (Kühl 1999). However, upon passing the 5 mm threshold, piezoresistivity no longer seems to occur. In essence it is sensitive to small bending, but unresponsive to large bending. It is also noted that upon releasing a PCB from bending back to a rest position, the resistance of the SMT tends to be higher than what it initially was. Resistance is also seen to change based on the orientation of the component. It is generally seen that face down mounted devices tended to have changes that were twice as significant as compared to the changes seen on face up devices (Kühl 1999). Usually, in face down components, the overall resistivity increased by about 0.25% whereas for face up, the net change was at maximum around 0.15% (Kühl 1999). Interestingly enough, the effect of piezoresistivity was seen to be independent of temperature fluctuations whereas in the situation of bending, it was "very linearly" affected (Kühl 1999). Temperature changes do cause, however, a change in the component itself. At high temperatures (~125 °C), we see a bending in a concave fashion and at low temperatures (~ -55 °C) an opposite effect is seen (Kühl 1999). The bending orientation is due to the thermal mismatch of the materials used in the component, causing the leads to deform

the package. At its most extreme, this causes cracks in both the component itself and in the solder joints, the latter usually being the most concerning. Kühl concluded that the overall deformation of a component must take into account all the deformations that occur, whether that is due to PCB bending, piezoresistivity or stresses resulted from either mounting or thermal expansions or contractions.

9.2.2. Side loads

In order to help ourselves in conducting our research on the thermo-mechanical reliability of SMT attachments our group decided that the best way to begin the research was by reviewing the relevant studies that have already been done on the topic in order to become as knowledgeable and up-to-date on the technology as possible. One of the useful sources that we came across was a paper titled "Solder Charge Grid Array: Advancements in the Technology of Surface Mount Area Array Solder Joint Attachment" (Hines, et al. 2011). In the paper the authors detail the advancements that SMT has helped create in technology, such as allowing for far more components to be placed in the same size circuit boards, thus allowing for smaller electronic devices. As more components get placed in smaller boards the reliability of components and the attachments increases as dependence on the devices that use them increases as does the difficulty in repair.

In their report, the researchers focus mainly on the reliability of SMT attachments in several different circuit board designs. The testing conducted by the researchers was conducted in accordance with test standards IPC-9701 (IPC 2002) as well as EIA-364-1000 (EIA 2000), both of which were very useful to our team in conducting our own testing. Each of the standards

includes numerous stress and temperature tests that give light to the overall reliability of the components both in short and long-term applications. One of the more interesting and important results that the researchers came across was the different stresses that can be handled by the current design of attachments in SMT. It was found that while current designs allow from loads up to roughly 5.85 lbs. of force when being pulled directly out of the board whereas the side loads per solder joint ranged from 0.041 lbs. per attachment to 0.417 lbs. per attachment (Hines, et al. 2011). It seems as if finding a way to increase the side loads that can be withstood by SMT attachments would be a good area for our group to focus on as there seems to be concern about the reliability of the components in this configuration.

9.2.3. Solder joints

To develop a better understanding on the thermo-mechanical reliability of SMT attachments, a look into the current state of SMTs is necessary. One helpful way this can be done is to look into relevant studies that have already been conducted on the subject. This allows us to know current and updated knowledge on the subject to aid us in our project. Since the reliability of SMTs is the key factor of this MQP, it was logical to look into the study on "SMT Solder Joint Reliability/Workmanship Environmental Test Results Correlation for LLC Assemblies" (Ghaffarian 1995). This study was done on the manufacturing process of leadless chip carriers (LLC) used by NASA, focused mainly on the soldering used to create them. Since soldering is the most common use of applying surface mount technologies to the given surfaces (boards, etc.) there will inevitably be failures that occur due to the soldering. This study highlighted some of the main soldering defects that can occur when SMTs are manufactured.

Through this study of LLCs, it became clear that the more prevalent defects that occurred involved “excess and lumpy solder” as well as “board contamination and grainy solder” (Ghaffarian 1995). The difficulty in problems such as these comes with how to effectively regulate these steps in the manufacturing process to bring failures to a minimum. One option suggested in this study was to increase the effectiveness of the quality inspectors who oversee the manufacturing of these LLCs. With more competent inspectors it is possible to recognize potential solder failures in the early stages of the manufacturing process. Earlier recognition of failures tends to lead to quicker solutions of problems overall. This study provided insight into one potential cause of SMT failures, soldering issues, which creates focus in this area. The more manufacturers read about soldering problems with SMTs, the more likely they will look into this stage of the process to correct for any errors. With more focus in this area of SMT manufacturing, there can be revolutionary changes in the field of creating SMTs. These changes can include new methods of solder usage within SMTs that can allow for both functionality and ease of production. Studies such as this shed light on aspects of SMT reliability that may not be considered as much as other sources of failure. When a more diverse range of failure options is investigated, reliability issues with SMTs can be diagnosed and correct quicker than ever before.

9.3. What issues did we focus on?

For our MQP we decided to do preliminary research into the types of testing that we could do to determine which SMT issues we deemed to be more important for the project given our limited resources. In our collective research, we were able to identify a few key issues that plague SMTs in general. While some issues were more prevalent than others, we thought it

necessary to understand the others as well to get a complete picture in terms of reliability assessment.

9.3.1. Thermal cycling

An issue not unique to just SMTs, yet still very damaging, thermal cycling is an issue that we planned to research and understand from day one. Thermal cycling is the process of cycling between a set of temperature extremes, usually at a relatively high number of cycles (over 1000 cycles with 1 cycle being 1 hour) (Kühl 1999). The constant heating, cooling and subsequent reheating of a sample under specific loads and conditions is a very effective simulator of life cycle and reliability.

Thermal cycle testing however can be very extensive and requires many samples to effectively test the reliability of a component given a set of conditions. It also is very costly so planning out a procedure beforehand is absolutely necessary (Ghaffarian, 1995). This would include testing such as rapid temperature change (over 2 °C/min), slow temperature changes (under 2 °C/min), among other things (Ghaffarian, 1995). However, we find that we can circumvent this issue by using computer simulation software, which can simulate conditions/environments in which components may be placed in. By modeling components in SolidWorks (Dassault Systèmes, 2013) and importing the CAD models into COMSOL (Littmarck and Saeidi, 2013), we can effectively simulate the failures that result from thermal cycle testing. From this we can then take our physical models and conduct testing that would give us the most interesting results as modeled by our COMSOL models.

To determine what would be good “temperature ranges” and “rates of fluctuation” we feel it best to contact companies like Watchfire Signs (Koebrich 2012) that have conducted

industry standard testing on their own boards. At the very least, choosing a standard that fits our time and resources is key. We don't require very broad temperature ranges, and certainly not ones that dip into the below freezing range (Ghaffarian, 1995). One of the approaches we have planned for physical testing is simply cutting certain sections out the boards we already have and subjecting them to different types of thermal cycling as per the COMSOL results (refer to section 10.4.1.2.). We expected most of our results to come from these simulations of thermal testing.

9.3.2. Power cycling

Another reliability issue test that we researched into was the use of power cycling. Power cycling is, in effect, the continuous cycling between on and off states for a component or set of components. This helps to simulate the life expectancy of the component(s) and is thus a great measurement for cycles to failure.

In terms of literature, there was not much documentation detailing the usage or process of implementing power cycling. We however were able to determine that because this would only be good for simulating aging effects, it would not be great for testing (Hedge, et al. 2008). As failures due to age are guaranteed for any SMT component, we realized that it would be more important to investigate the issues that aren't guaranteed in an attempt to mitigate them (Hedge, et al. 2008). These include: thermal cycling failures, failures due to vibrational effects, and issues concerning the material properties of the components. Given the limited amount of testing samples we were able to obtain, the fact that we don't have the proper power source for these samples, and the fact that we would need to develop our method that would effectively fluctuate power to the board at an arbitrarily chosen constant rate seemed like more trouble than it was

worth; especially when compared to the results that thermal cycling and vibrational testing were likely to give us (Hedge, et al. 2008). In the interest of time, we have currently decided to put further investigation and testing with regards to power cycling on hold, subject to whether we get more boards, time constraints, outside company help, etc.

9.3.3. Vibrational

Vibrational testing with regards to SMTs is basically the testing of how SMTs react to vibrations over 150 Hz while in use (Blattau, 2012). From a perspective of vibrational issues, this issue serves to reinforce the fact that a heavy analysis should be placed on the solder as compared to the SMT attachments themselves. In most cases, during High Cycle Fatigue (HCF) tests (~150 Hz for over 1000 cycles), failures occur in the lead or solder joint (Blattau, 2012).

When it comes to small SMT components, there seemed to be little to no effect on the attachments whatsoever under these vibration frequencies. SMTs only seemed to suffer when the component itself was large. These issues tend to usually be cracking in the solder itself or cracking of the chip carrier itself due to warping in the board caused by the vibrations. In the case of large components, one of the solutions that manufacturers have taken to solve this issue is by “anchoring” the attachments with a glob of silicon around the solder joints themselves (Blattau, 2012). Another solution that other manufacturers use is the utilization of ceramic quad flat pack (CQFP). The CQFP helps to mitigate 2 different types of issues in one package. First, the CQFP includes a heat sink that helps to lower the impact of temperature on the package, as well as thermal paste to distribute heat evenly. Second, the CQFP helps to anchor a package, thus making it less susceptible to vibrations (Actel, 2003).

There is no actual solution in terms of dealing with damaged components other than making the components smaller which is what manufacturers are trending towards anyway. Vibrational failures tend to manifest in the board and joints rather than in the SMT components themselves. When the attachments are large, these vibrational effects become more prominent.

By keeping leads small and stiff, manufacturers increase the chances of SMT components staying on the board. As opposed to thermal cycle simulation on components, vibrational computer simulations on the components themselves will not produce any substantial results. The actual effects due to vibration would only be visible with a model of the entire board and all of the components. Observing the vibrational effects over an entire board would allow us to accurately discern the stresses imposed on individual components on the PCB as a whole.

9.3.4. Materials issues

One important consideration when dealing with surface mount components is the material interaction between the component leads, the solder, and the PCB copper pad. The most commonly used soldering material is a Tin-Lead alloy (Sn-Pb) (Tu, et al. 1997). When Sn-Pb solder contacts the copper pad, intermetallic compounds (IMC) are formed between solder and pad. The molten solder reacts with the copper pad to form a Cu-Sn intermetallic species (there are various phases of the Cu-Sn compound present in the IMC). These phases are the Cu-Sn Epsilon-phase or Cu3Sn, and the Cu-Sn Eta-phase or Cu6Sn5 (Tu, et al. 1997). The IMC serves as bonding material for the solder joints.

Thickness of this IMC layer is heavily dependent on reflow time and temperature during soldering. The reliability and performance of solder joints are tied to the size of the IMC layer. A

very thick IMC layer results in premature mechanical failure in the operating environment such as power and thermal cycling (Tu, et al. 1997). An increase of Cu6Sn5 phase in the IMC reduces mechanical strength (ability to withstand stresses) at the solder joint interface. An increase in thickness of IMC Cu3Sn from 0.7 to 1.3 micrometers shows an increase in the shear force required to fracture the solder by about 20%. Which shows that the IMC effect on reliability is complicated, since it can both decrease and increase reliability of the joint (Tu, et al. 1997).

As mentioned, the thickness of the intermetallic compound layer can have a positive effect on solder joint strength. The thinner the IMC layer, the greater the number of cycles to failure a solder joint can withstand. The growth of the IMC is controlled by the amount of reflow time when preparing the solder. Solder joints cannot be formed successfully when reflow time is less than 20 seconds. However, with a reflow time of 20 seconds, an IMC of 0.95 micrometers thick can be achieved. This thickness has shown to yield the highest reliability and the greatest number of cycles to failure in laboratory testing. Longer reflow time leads to higher IMC layer thickness, which has an adverse effect in the lifetime of the joint. But longer reflow time also leads to rougher interface, which increases joint performance (Tu, et al. 1997). The uneven rougher surface tends to be more shear resistant than the flat IMC layer. An increase in IMC layer thickness from 0.95 to 1.4 micrometers decreases the lifetime of the joint. After the 1.4 micrometer threshold is reached, the positive effect of the rough surface created by the thicker IMC overcomes the weakening of the joint. The joint will still not be as reliable as a thinner IMC layer, but the decrease in reliability is less significant for thicknesses greater than 1.4 micrometer than from 0.95 to 1.4 micrometers (Tu, et al. 1997).

The Cu3Sn phase is formed as a result of the thermal cycling of the solder joint interface. When the solder has been applied to the joint, only the Cu6Sn5 phase is present. As the component is thermally cycled, the epsilon-phase grows in the IMC. The epsilon phase has the advantage that cracks don't form or propagate at the grain boundaries. On the contrary, the eta-phase of the IMC is directly responsible for crack formation and failure of the solder joint. Monitoring of the reflow time and thermal cycles is key to ensure a reliable and long lasting solder joint, since these parameters affect the development of IMC layer, which is the site for most material based failures in surface mount components (Tu, et al. 1997).

9.3.4.1. Material analysis

SMTs have become a staple of the electronic circuit industry. The ability to place components in the surface of the printed circuit board, allows for greater packing density when compared to more traditional through-hole components. With more and more SMTs being found in electronic devices, cars, and airplanes, it is important for these components to be reliable. The reliability of the component is tied to the materials used in its manufacturing. Therefore, it is important to choose the appropriate material to prevent premature failure. Some of the common issues that arise in SMT industry have much to do with the thermal stresses experienced by the cyclic loading that occurs through the components lifetime. Despite careful considerations from engineers and scientist, failure is bound to occur. Whether this is due to cracks at the joint surfaces, or as result of poor thermal management, there are several issues faced by those in the industry.

There are various material properties that have to be taken into account when choosing the right material for a SMT. Thermal expansion coefficient in particular requires a great deal of

attention. Components heat up as current flows through them; this in turn leads to the materials of the component expanding resulting in thermal stresses. The yield strength of the materials then comes into play. If this parameter is exceeded by the thermal stresses, then the component would plastically deform and ultimately lead to failure. In order to prevent premature failure due to thermal stresses, high importance is given to the material selection process.

Surface mount components used a variety of materials. They are complex systems compromising of metals, polymers, and ceramics. Due to their dynamic nature, it is important for designers and engineers to correctly select materials that not only provide the desired functionality, but are also able to withstand the stresses and loads they are subjected to during the SMT's lifetime. Intel, one of the leading manufacturers of electronic components and IC chips, release a component packaging databook, in which they detail some of the most commonly utilized materials in the industry. These tables can be found in Appendix A.

10. Methodology

10.1. Approaching the issues

For the purpose of this MQP, we were aware that we needed to acquire more information on the current state of SMTs and their issues. We decided it would be best to try to contact companies and industry leaders in an attempt to learn more information on how these companies utilize SMTs, what they do about issues, and what future they see for SMTs. In addition, we decided that observing these issues first hand was critical to our understanding of SMTs. We concluded that computational modeling was beneficial as an observational approach. From this modeling we were able to produce to computational analysis of the issues with regards to SMTs.

10.2. Manufacturer information

As previously stated, our group was interested in acquiring information regarding current SMT issues, and the methods in which companies mitigate them. Paired with this information, we also sought to obtain PCB samples from manufacturers to accurately model components for computational analysis.

10.2.1. Contacting industry leaders

The group determined that a list of companies and contacts was needed to obtain information and samples. This list was first compiled through researching companies that had any connections with SMTs. This research led us to discovering *smtnet*, a website devoted to companies involved with SMTs. From this website we were able to refine our preferred list of companies to contact, by focusing on companies involved in the testing, packaging, and

manufacturing of SMTs. Through this list we were able to acquire company emails and contact information that allowed us to be in contact with executives of each company. We sent each company a description of our project and a questionnaire that asked for specific information that we felt would further our knowledge of SMT (questionnaire found in Appendix B).

10.2.2. Response from industry leaders

The overall response from industry leaders did not meet the expectations that the group had when first setting out to contact these companies. Out of the over 25 companies contacted, our group only received a significant response from one company, *Watchfire Signs*, an LED sign company located in Illinois (Koebrich 2012). Through emails and an eventual conference call with the Vice-President of Engineering, Jeff Koebrich, we were able to obtain some information addressing *Watchfire's* concerns and outlooks regarding SMTs. Mr. Koebrich informed us that of all failures that affect SMT, thermo-cycling issues leading to solder joint failures are the most common issue plaguing the industry.

10.2.3. Reaction to industry response

After receiving minimal response from industry leaders in SMT, our group felt it necessary to reformulate our approach to the overall problem. We were no longer going to be able to be influenced by what information and samples we received from these companies, as there was virtually nothing to work with. Due to this lack of response, it was imperative that we looked elsewhere to obtain parts for any potential modeling and testing. Our group was fortunate enough to receive two PCBs that were developed by Foxconn through an employee of BGRIMM (Xiao 2013). With these boards, we now had the ability to reference our models after. The introduction of these boards also allowed us to follow the path of computer modeling as a

primary source of data acquisition as it was both faster and more available to the group. Using the newly acquired boards, we were able to create and test models that were based on actual components, rather than creating components ourselves.

10.3. Determining appropriate software

One of the MQP's main objectives was to conduct a finite element analysis of a surface mount component. There is a variety of commercially available software that is capable of conducting this type of analysis (Pryputniewicz, et al. 2001). Finite element analysis works by taking a defined system and dividing it into a series of connected smaller systems, to evaluate an equation or set of equations at these smaller points (Pryputniewicz, R. J., et al. 2002). These smaller systems can easily be solved using a simplified approach and approximations. This in turn can yield a set of solution for the whole system, with accuracy proportional to the number of elements used in the discretization of the result (Pryputniewicz, D.R., et al. 2002). Finite element analysis (FEA) is widely used in the contemporary industry to solve all kinds of problems. Whether it is thermo-fluid related, mechanically related, or both, FEA is a useful tool in the analysis of complex systems (Pryputniewicz, et al. 2003). Therefore, conducting this type of analysis is essential for the project to obtain meaningful results (Pryputniewicz and Stupnicki 1994).

10.3.1. Choosing specific software

The process of selecting the appropriate software to conduct the FEA was a relatively easy one. The first step was to look at the most commonly used FEA software in the engineering industry. From this research, we found that ANSYS Workbench, SolidWorks simulation, and

COMSOL Multiphysics, were some of the more vastly utilized FEA computer programs. One of our team members had previous experience with the use of ANSYS, thus leading us to originally choose ANSYS as our default software for the FEA.

Around January 2013, we were informed of a demonstration on the computational capabilities of the FEA software COMSOL Multiphysics. We knew little about this program, but we were advised to attend the demonstration and expand our knowledge of finite element computational methods. This demonstration proved helpful and led us to switch from ANSYS to COMSOL as our default analysis software. COMSOL's various physics modules, its material library, and its particular interface made it the right candidate for the thermo-mechanical analysis of a surface mount component.

10.3.2. Software capabilities

The demonstration of COMSOL Multiphysics was the deciding factor on selecting the software for the FEA. The two modules within COMSOL that are of particular interest for this MQP are the Joule Heating, and the Solid Mechanics modules. These modules allow us to simulate the thermo-mechanical conditions to which SMTs are commonly subjected to. Fortunately, COMSOL Multiphysics is available through WPI's software services, providing our group with more of an incentive to utilize this software. In order to gain a better understanding of COMSOL, we developed a test model of a J-lead surface mount component based on the 24 Lead Small Out-Line Package (SOJ) Variation: J-lead geometry obtained from the Intel packaging databook (Package/Module/PC Card outlines and dimensions) (Intel, Ch. 2, 2013). Only a quarter of the component was modeled because of symmetry and the increased speed of

calculation. Figure 1 shows the resulting 3D geometry constructed using SolidWorks.

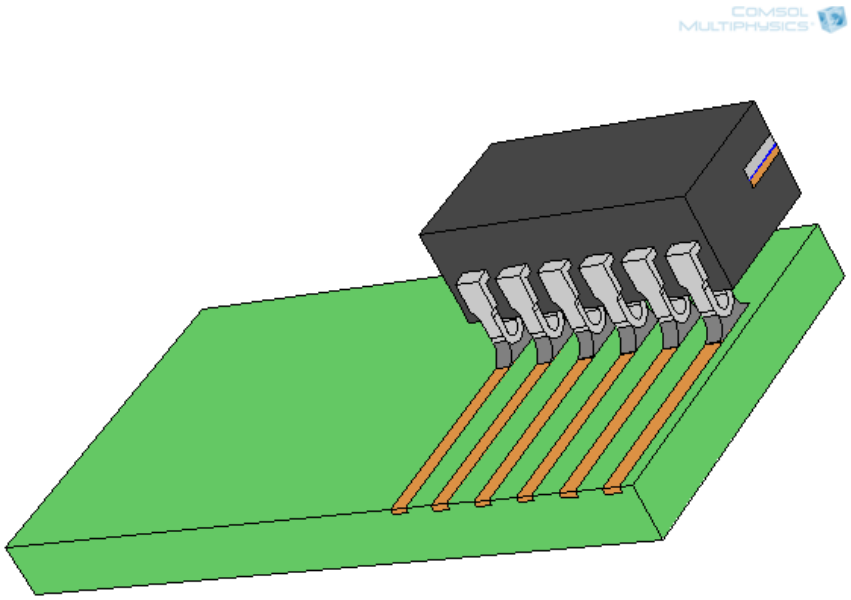

Figure 1. Image showing a quarter (because of symmetry) of a surface mounted J-lead chip carrier on a PCB.

Once the model geometry was completed, the next step was assigning the materials to each of the different parts. In order to conduct an accurate analysis, it was important to correctly define the material properties of the modeled SMT. Using the tables located in Appendix C; we were able to determine the materials needed to characterize the component (Intel, Ch. 5, 2013). The majority of this material information was found within the material library of the COMSOL Multiphysics software. The remaining values were obtained from the CES Edupack software which offers a variety of material properties that would otherwise be difficult to obtain (Ashby and Cebon, 2013). Using these materials and properties, Table 1 shows the materials selected:

Table 1. Table listing the material employed to define the model used for FEA.

Part	**Material**
PCB	FR-4
Cu-wire:	Copper (Cu)
J-lead	Aluminum (Al)
Solder	60Sn-40Pb
Chip-Carrier	Polyimide
Wire frame:	Copper (Cu)
Chip	Silicon (c)
Die attach	Ag filled Epoxy

Now that the materials have been assigned, the physics modules can be selected.

The first module is Joule Heating. The Joule Heating multiphysics interface combines the Electric Currents and the Heat Transfer interfaces for modeling of Joule heating (resistive heating). This condition is applied all through the model; however, specific boundary conditions need to be set as well. The first set of boundary conditions are the terminal and ground conditions. For the terminal condition, voltage was selected as the terminal type and an electric potential of 0.01 V was used to perform the analysis (Analog Devices, 2008). The terminal is applied to the first Cu-wire surface, and the ground is applied to the last Cu-wire. Figure 2 illustrates the placement of these boundaries.

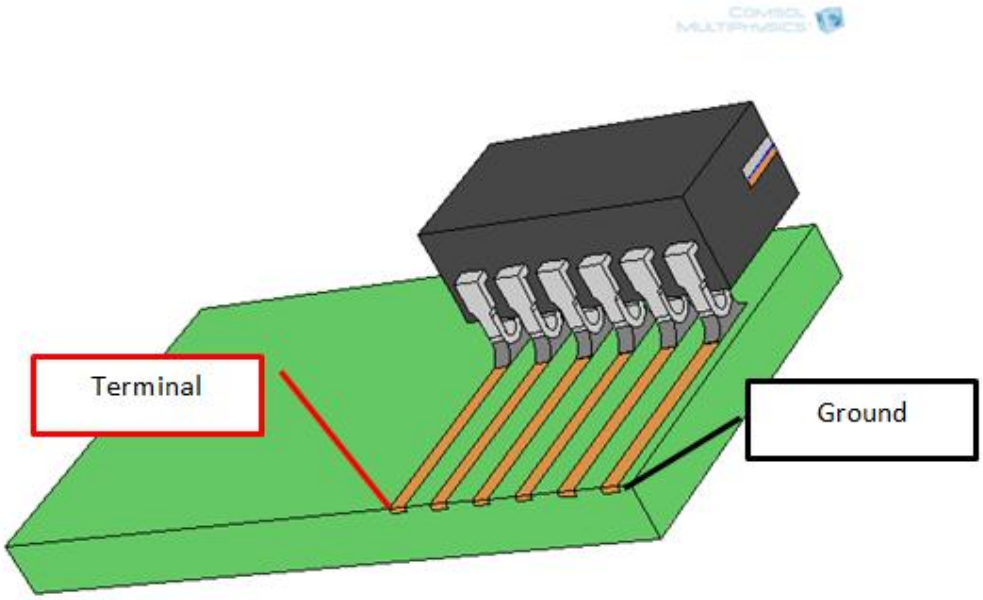

Figure 2. Test model showing the placement of the terminal and ground boundary conditions.

Next was the addition of inward heat flux and convective cooling boundary conditions. These two conditions add the effect of natural convection into the system. A convective coefficient of 5 W/m^2-K was selected since this value closely resembles the coefficient of still air (Incropera and DeWitt, 2007). For the initial values, a starting temperature of 293.15 K (0°C) and an electric potential of 0 V were assumed. We applied the voltage at time t=0, not as an initial condition, but as a loading condition. The module also includes other default boundary conditions that were left untouched.

After finishing the Joule Heating module set-up, the next step was setting up the Solid Mechanics module. The Solid Mechanics interface has the equations and features for stress analysis and general linear and nonlinear solid mechanics, which solve for displacements. The Linear Elastic Material is the default material, which adds a linear elastic equation for the displacements and has a settings window to define the elastic material properties. From the

Linear Elastic Material condition, a Thermal Expansion condition was added to the entire model. The reference temperatures for the expansion condition were the initial temperature of 293.15 K and the resulting temperatures from the Joule Heating module. A fixed constrain condition was added to the bottom of the PCB since it is assumed the bottom of the board is fixed in place during the analysis. Once all of these conditions are selected, the physics tree should look like Figure 3.

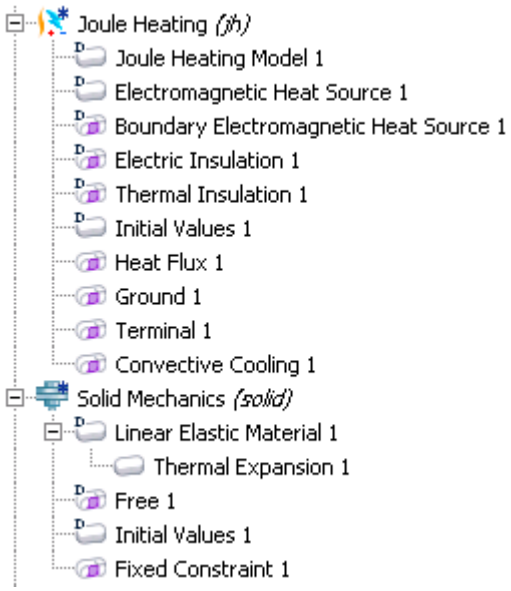

Figure 3. The physics module tree showing the selected modules and respective boundary conditions applied to the FEA.

The following step is to create the mesh for the finite analysis. COMSOL allows the user to either manually create the mesh, or allow the physics interface to do so. For simplicity sake, the latter was chosen. The physics-controlled mesh options allow COMSOL Multiphysics to create a mesh that is adapted to the current physics settings in the model. The overall element size of the physics-induced mesh can be changed by selecting a new element size setting in the Element size list, which rebuilds the mesh. Figure 4 shows the physics-generated mesh. It should be noted the size of the elements varies with the size of the domain. This allows every domain to

have a proportional number of elements corresponding to their overall size.

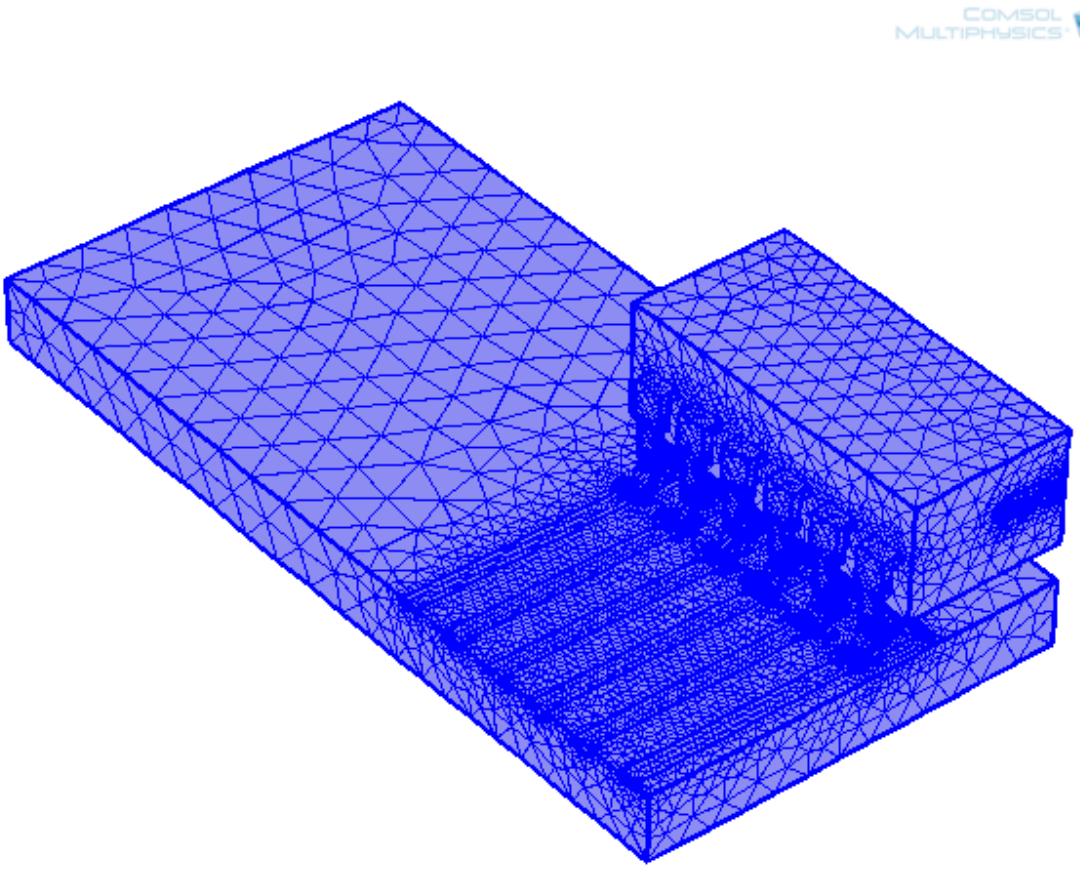

Figure 4. Physics-generated tetrahedral mesh of the j-lead surface mounted component.

The last step in the process is to conduct the study itself. The study consisted of two stationary steps; the first solving the Joule Heating condition, while the second utilizes the solution of step 1 to calculate the Solid Mechanics condition. Once the steps were establish, the study then proceeded to compute and solve for the temperature and resulting von Mises stresses. The computational time varies with the complexity of the model. For the test model, COMSOL took approximately 17 minutes and 21 seconds to complete the calculations. It solved for 509,472 degrees of freedom for the Joule Heating step, and 764,208 degrees of freedom for the

Solid Mechanics step. Since the meshing is controlled by the physics of the program, COMSOL adjusts the number of elements in order to converge on an appropriate solution. Now that the calculations were completed, we were able to look at the temperature and stress distributions.

Figure 5 shows the resulting temperature distribution throughout the component as a result of the 0.01 V voltage potential load. The highest temperature is found at the lead where the voltage potential load was applied. The average temperature throughout the chip carrier was of 298.5 K. The average temperature throughout the PCB was of 296.2 K, with temperatures near the leads being of about 298 K. The ambient temperature for the analysis was 293.15 K as mentioned before.

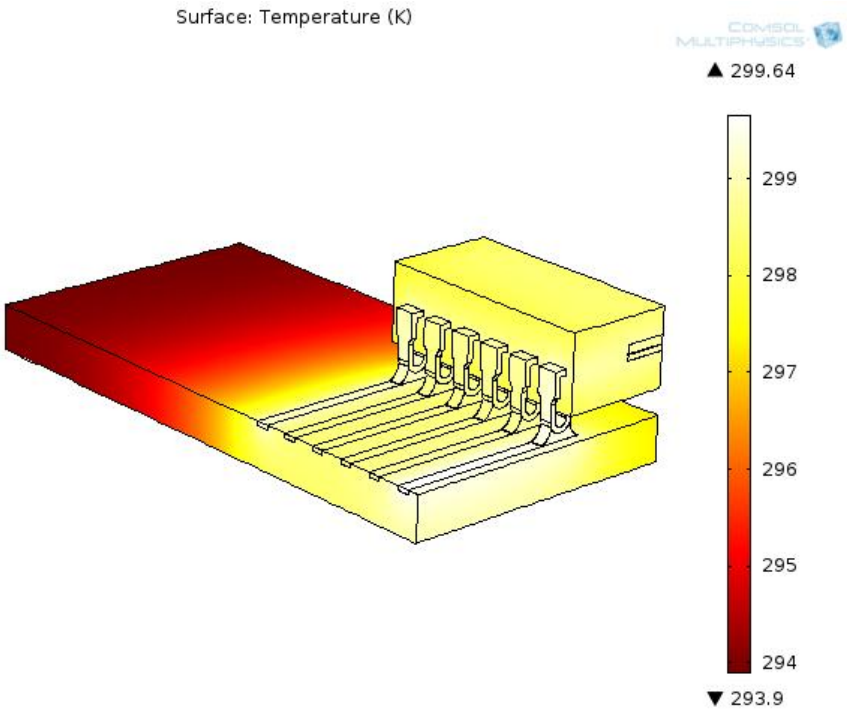

Figure 5. Surface temperature (K) distribution throughout the model when a load of 0.01V is applied.

Figure 6 shows the resulting von Mises stress calculated by the FEA. The Von Mises stresses (MPa) are a representation of the total stresses that result from the mismatch in thermal

expansion coefficients of the materials in the chip carrier when heated by the applied voltage. The added heat leads the material to expand and cause stress within the different parts of the model. It can be seen in the image below that the highest concentration of stresses happens at the Cu-wires and Silicon chip interface.

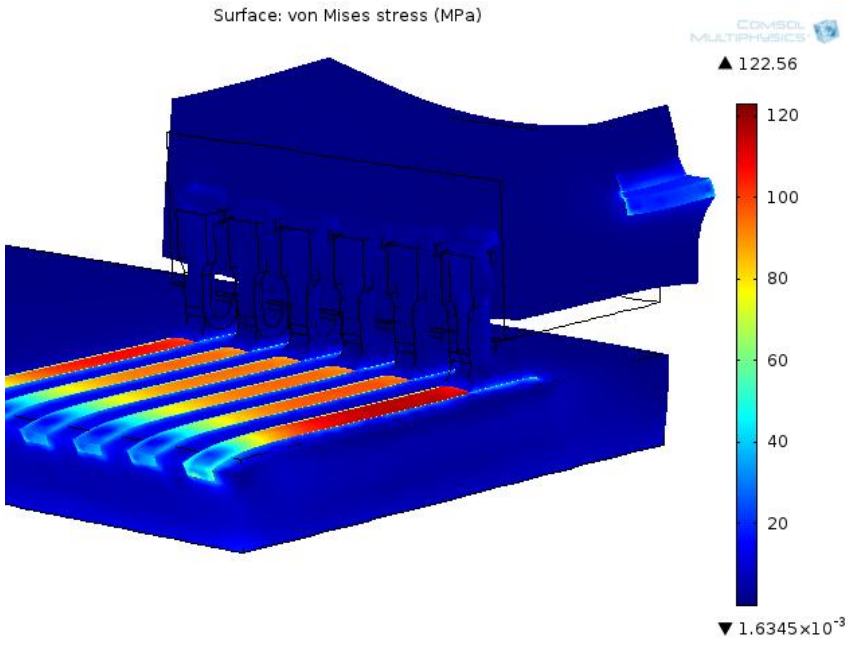

Figure 6. Resulting von Mises (MPa) stresses under the Joule heat load of 0.01V for the test model.

The Cu-wire stress can be ignored since for simplicity of the model, their size was largely exaggerated. There's also a noticeable deformation in the chip-carrier as a result of the thermal stresses that occur when the component is under the load of the voltage. The average von Mises stresses at the solder can be calculated with the help of COMSOL. For this particular model, the stress at the solder was of 4.31 MPa. This value is well below the yield strength of 35 MPa for 60Sn-40Pb solder, which means the component would not fail under the 0.01 V load.

10.4. Discussion of components

10.4.1. AD623 chip

To acquire a full understanding of this specific component (AD623 Chip), we found it necessary to utilize two types of software: SolidWorks and COMSOL Multiphysics (Analog Devices, 2008). We planned to use SolidWorks to create the model, while using COMSOL to perform the desired tests and computational analysis.

10.4.1.1. SolidWorks model

To create the models we began by looking at the PCBs that we had and identifying the different SMT components on the boards based on the identification numbers on each component. We ran into quite some difficulty in trying to find datasheets for each of the components due to vague identification numbers, as well as a lack of reliable resources. We were able to identify one as an amplifier produced by *Analog Devices* called AD623. Through the use of further Google searches we were able to find the datasheet for AD623 (listed in Appendix D) which assisted us in producing a model of the component (Analog Devices, 2008).

Similarly to the initial model we made, we created the AD623 model first by creating the leads and the solder attachments for them. However, in this case the leads were gullwing style as opposed to J-lead (Analog Devices, 2008). Once again, we created the chip carrier with three separate rectangular layers of material mated together; Figure 7 shows the full model as seen in SolidWorks.

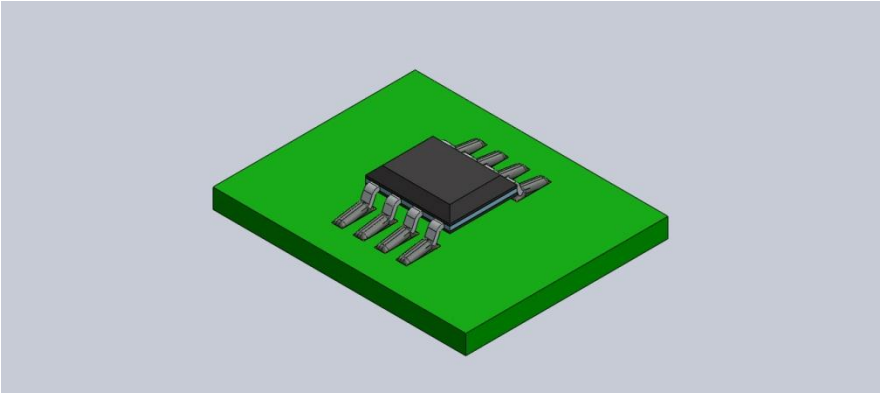

Figure 7. AD623 SolidWorks chip carrier model (black).

In the assembly stage we used several types of mates to join the different components of the model. We began by creating an assembly consisting of just the J-Leads and the solder, with solder on both regions of the underside of the J-lead. After that, we created an assembly that began by mating the extruded rectangles that make up the package and then imported copies of the J-lead/solder assembly into the final assembly. We then mated the top part of each J-lead/solder assembly to the extruded rectangles. Once the model was done we were able to move on to COMSOL.

10.4.1.2. COMSOL model

After the SolidWorks model was created, it was imported into COMSOL Multiphysics. We assigned material properties to each element: PC board as FR4 (circuit board), solder as Solder 60Sn-40Pb, leads as Aluminum, middle layer of chip as silicon(solid, bulk), lower layer of chip as Copper, upper layer of chip as acrylic plastic.

Each lead was assigned to experience a 2 mV drop, with the quartered chip consuming 0.125 W of power. The generated heat is conducted within the model and is cooled on the surface by the air. Once the mesh and study steps we set, a temperature profile was generated.

From the thermal expansion coefficient embedded in properties, we can also find stress. The highest temperature is at the chip, and highest stress is in the region of silicon layer. Figure 8 provides information of temperature for our quartered model. This plot shows that the chip has higher temperature (27.8 °C). The pc board has lower temperature, ranging from 26 to 27 °C.

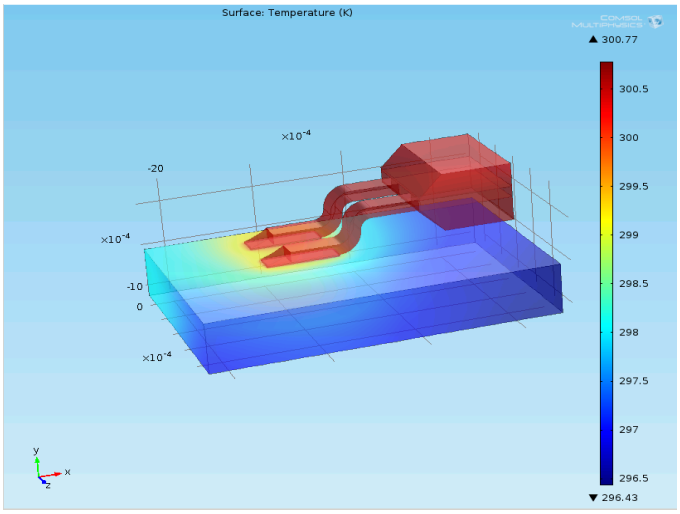

Figure 8. Temperature profile.

Figure 9 shows how heat is transferred within the model. Since the primary heat source is the chip, the majority of the heat is conducted through the J-lead to the PCB. Along with convective cooling from the air, the heat generation creates temperature difference that is shown in Figure 8.

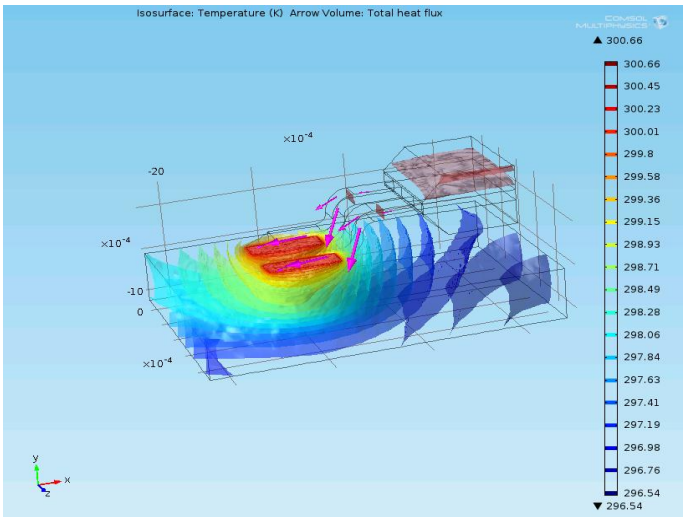

Figure 9. Temperature contour and arrow volume.

Figure 10 shows the Von Mises stress in our model. The magnitude of stress is highest in silicon substrate, around $2*10^7$ Pa. The stress in J lead is relatively low, with around $1.3*10^7$ Pa.

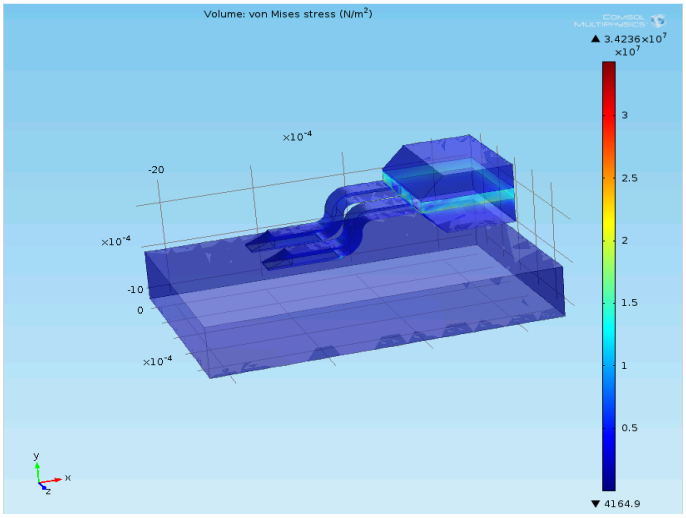

Figure 10. Von mises stress.

10.4.1.3. Uncertainty analysis

To ensure that what we are testing with had a proper uncertainty range, we created an uncertainty analysis model in MathCad. Using our prior knowledge of uncertainty analysis, we were able to determine what variables were necessary to calculate uncertainty. These variables included temperature and material properties, which led us to determining the uncertainty percentage contributions of each factor to the total uncertainty. Some uncertainties were assumed as the exact values could not be determined through conventional means. Utilizing MathCad's capabilities, we were able to determine the desired uncertainties to ensure that they fell below one percent. Through analysis of the MathCad solutions, we concluded that the largest contributor to uncertainty was the 'e' factor, a material property used for calculations at ambient temperature.

10.5. Experiment preparation

To develop a further understanding of the computational results that we obtained through COMSOL, we decided to physically test the components as well. Testing the components allowed us to develop overall results that were more substantial that the one-dimensional results obtained only through the computer modeling. We were able to compare the results of our testing with those from the computer simulations to reinforce any conclusions that we made regarding the reliability of the SMT components. The simplistic nature of the Foxconn boards provided for easier testing procedures, and an overall easier testing process.

11. Experimental information

11.1 Materials used

Our group was fortunate enough to have access to labs around the Worcester Polytechnic Institute (WPI) campus. We utilized one such lab to perform tests on the Foxconn-developed boards that we acquired. The experiment was conducted in WPI's Higgins Laboratories under the guidance of the laboratory manager Peter Hefti. Along with the boards themselves, we utilized additional equipment to effectively test the AD623 chip. For the experiment we needed: a power supply to provide voltage to the component, a single thermocouple to measure the chip temperature, thermal paste to fashion the thermocouple to the chip, a multimeter to ensure the correct voltages were being used, and wires to connect all of the parts to the appropriate locations.

11.2 Experimental procedure

The purpose of this experiment was to test how much the temperature changed for the AD623 chip when comparing the nonoperational temperature to the operational (steady state) temperature. To allow the retrieval of this measurement, a wire was first soldered to the negative power supply in order to power the component. Figure 11 depicts the full layout of the experiment.

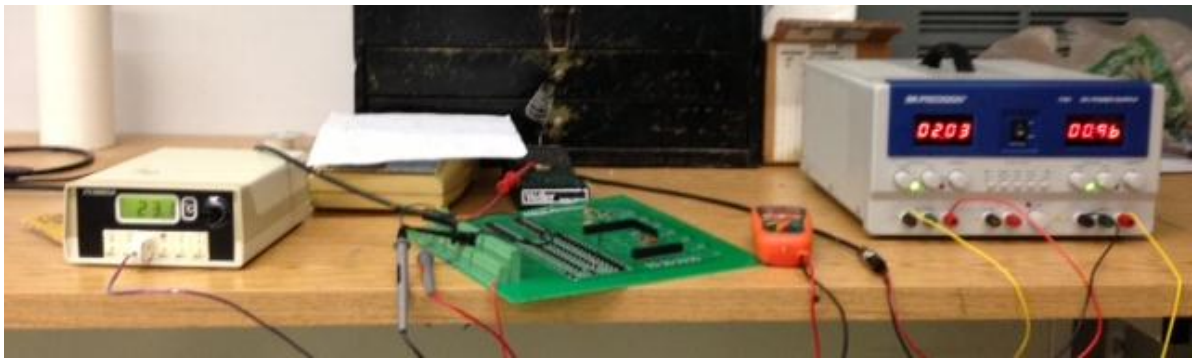

Figure 11. Experimental set-up to measure SMT temperature.

For this particular component we used two voltages: + 2.5 V and - 2.5 V for the voltage supply, and 1 V for the input from the voltage supplier (Analog Devices, 2008). In total, a 9.34 V difference occurred between the amplifier's output and ground. The thermocouple was first used to measure the ambient air temperature, as this was determined to be the nonoperational temperature for the chip. After averaging separate measurements, the nonoperational temperature was determined to be around 20.5 °C. Once this base value was determined, we applied the voltage to the chip in order to power it up. Before the temperature of the chip was measured a second time, a period of around five minutes passed so that a steady state could be reached, and accurate readings could be obtained. The thermocouple needed to be attached to the chip, using thermal paste, in order to record the surface temperature during the steady state. Figure 12 illustrates the thermocouple attached to the chip with the thermal paste, as the thermal paste allows for more accurate results.

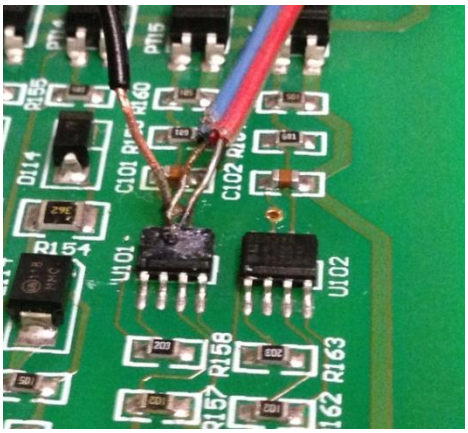

Figure 12. Thermocouple measuring the AD623 chip temperature.

Once the chip was powered up and reached a steady state, the thermocouple measured the operational temperature of the chip. Using the measured temperature change, we were able to compare the experimental change with the change calculated in COMSOL to verify that the COMSOL models were useable.

12. Results and discussion

12.1. Experimental data

Once the chip reached its steady state, the surface temperature of the chip was measured to be 28 °C. Figure 13 shows the displayed thermocouple reading of the chip's operational temperature.

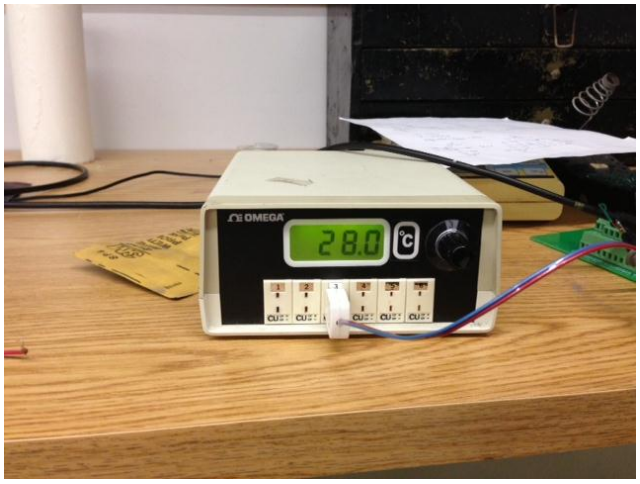

Figure 13. Operational temperature of the AD623 chip.

To replicate the computer modeling, we also measured the temperature of the PCB immediately surrounding the chip. The computer models included a small section of PCB around the chip in its calculations, so it was necessary for us to do the same in the experiment in order to have consistent measurements. The temperature measured around the chip was found to be 27.5 °C, and is displayed in Figure 14.

Figure 14. PCB temperature during chip's steady state.

These values were used to further define the uncertainty for the AD623 chip. The experimental results are also significant in validating the results obtained from the COMSOL simulations.

12.2. Connections to methodology material

12.2.1. Connections to COMSOL data

One of the project's main objectives was the use of finite element analysis as a tool to explore the thermo-mechanical behavior of surface mounted components. FEA is a powerful tool that can provide valuable information, however, it relies upon ideal conditions and user inputs, and it requires some sort of experimental validation. The aforementioned experimental temperature measurements of the AD623 component were utilized to validate the FEA.

In order to achieve a correlation between the FEA and the experimental results, input variables for the FEA were adjusted as needed. One of the particular parameters that was adjusted was the convective heat transfer coefficient. The value for convective heat transfer can

be calculated using various relationships and parameters such as the Nusselt number. The value of this convective coefficient varies anywhere from 2 to 25 W/m^2-K for air at an ambient temperature of 20 °C (Incropera and DeWitt. 2007). A value of 10 W/m^2-K was utilized in our analysis because this value allowed the COMSOL analysis to yield a similar temperature response to that of the experiment. Once a temperature correlation between the FEA and the experiment was achieved, further analyses were carried out.

The COMSOL analysis provided valuable data for the AD chip under a voltage load. Figure 15 shows the temperature response of the quarter model that was analyzed. It can be seen that the highest temperatures are found in the leads and solder of the component. The average temperature for these components was 29.23 °C. It can also be seen that the temperature varies through the PCB, with the highest temperature located near the leads. The average temperature for the PCB was found to be 25.48 °C, compared to the 27.5 °C measurement exhibited in the experiment. The Chip-Carrier exhibited an average temperature of 29.02 °C, compared to the 28 °C measurement exhibited in the experiment. These values were utilized to conduct further analyses.

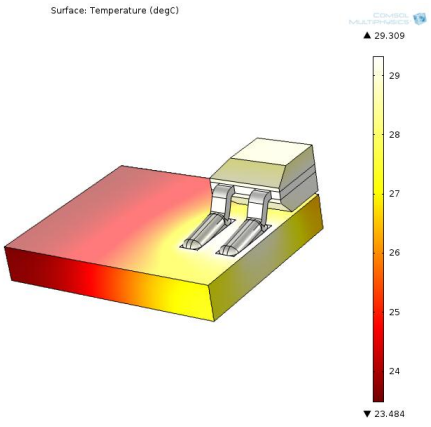

Figure 15. Temperature distribution of component.

Figure 16 shows the von Mises stress criterion distribution of the SMD. The von Mises stress tells whether or not the component will fail due to stresses at the solder. From COMSOL, the average von Mises stress at the solder was 1.436 MPa. A cross section of the solder was also examined in order to look for a more exact stress concentration of the solder.

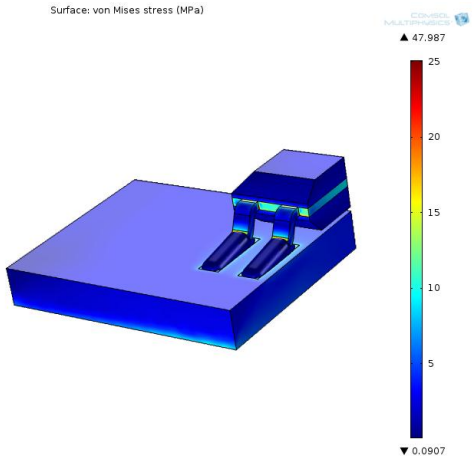

Figure 16. von Mises stress distribution of component.

Figure 17 shows this cross-section and the corresponding von Mises stresses. Here it can be seen that the solder experiences stresses around 5MPa near the interface of the lead. However, this value is most likely exaggerated due to the nature of the geometry used for the modeling.

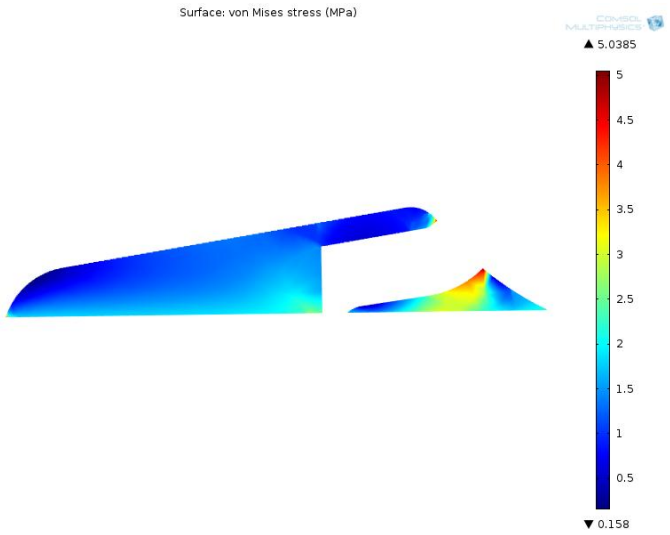

Figure 17. von Mises stress distribution of cross-section of solder.

The thermal strain response of the SMD was also obtained from through FEA analysis. Figure 18 shows the thermal strain distribution through the device. It can be seen from this figure that the highest thermal strain is experienced by the chip carrier. This result is expected due to the chip carrier having the highest coefficient of thermal expansion out of the materials that make up the component.

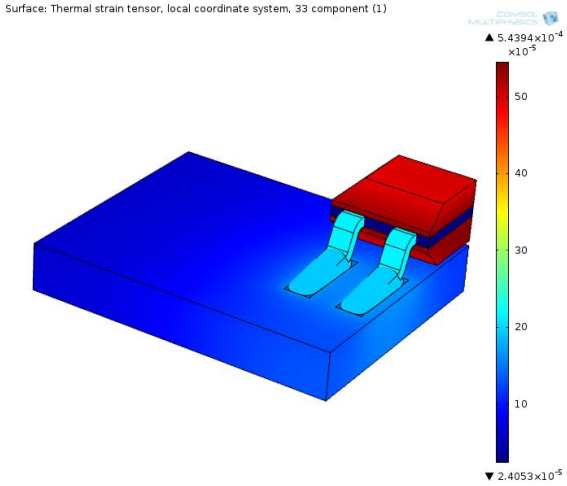

Figure 18. Thermal strain distribution of component.

Lastly, the temperature distribution and heat flux can also be observed with the help of the COMSOL analysis. Figure 19 shows the iso-contours temperature distribution throughout the mounted component and PCB. The total heat flux can be seen in the form of arrows, where the size of the arrow denotes the magnitude of the flux.

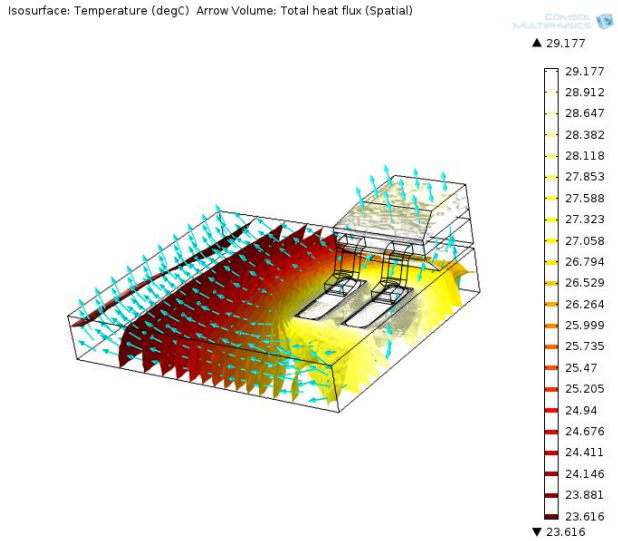

Figure 19. Temperature iso-contours & heat flux of component.

COMSOL allows the full view of the component FEA results using the 3D mirror view. This option as seen in Figure 20 is under the Data Sets portion of the hierarchical tree of the COMSOL interface. With this view, full renditions of the steady state results can be observed.

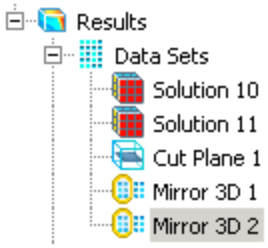

Figure 20. Hierarchical tree showing the Mirror 3D option.

Figure 21 shows the temperature distribution of the component.

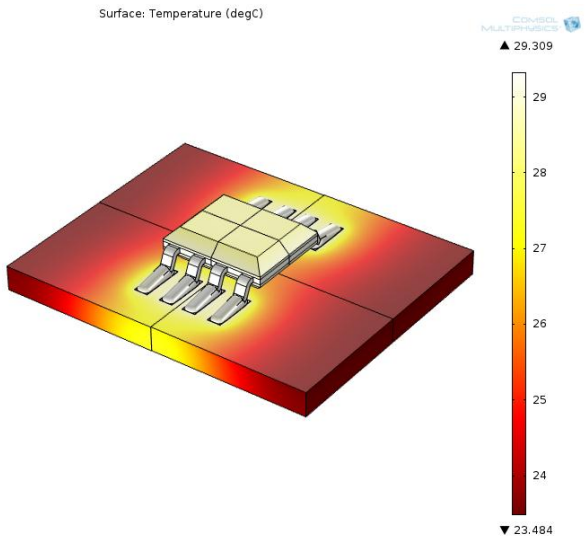

Figure 21. Temperature distribution of entire component.

Figure 22 shows the von Mises stress criterion.

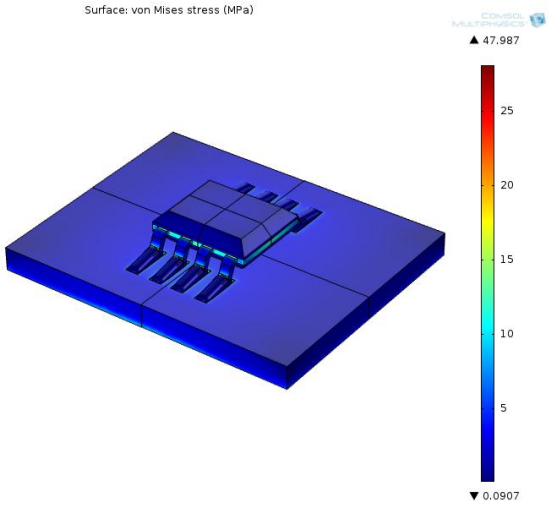

Figure 22. von Mises distribution of entire component.

Figure 23 shows the thermal strain induced by the temperature change.

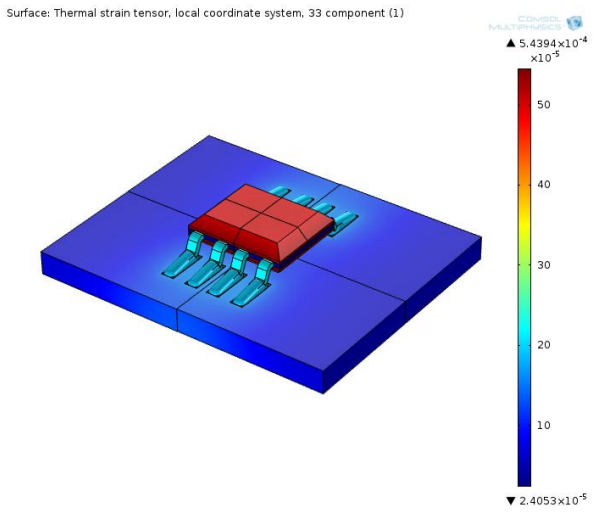

Figure 23. Thermal strain distribution of entire component.

COMSOL multiphysics also provides the option to run a transient analysis. A transient analysis was run for a total of 750 seconds. Through several trials, it was determined that 750 seconds was the appropriate time to run the transient analysis in order to reach the steady state results that are shown above. The transient analysis was conducted to better understand the component's response over 1 power-up cycle. This analysis yielded data for temperature, von Mises stresses, and thermal strain over time. This data was then exported from COMSOL as a comma separated value (CSV) file that was then imported into MathCad for further analysis.

The data extracted from the transient analysis was the average of all the values within the specific volume. Meaning that all the temperatures, stresses, and strains found in each specific component (chip carrier, PCB, solder) were averaged out to obtain a finite value. Using MathCad the data was further analyzed to yield the following results and graphs. From literature, we

obtained the following equations which were instrumental in carrying out the analysis (Pryputniewicz, 2013).

- Mean solder temperature (T_{sm}): This equation allows the solder to be treated as a finite element. It is one of the parameters used for the selection of the appropriate fatigue ductility coefficient and fatigue ductility exponent in the Mason-Coffin fatigue life equation. This equation utilizes the ambient temperature (T_{amb}), the printed circuit board (T_{PCB}), and the chip carrier temperature (T_{cc}).

$$T_{sm} := \frac{1}{4}\cdot\left(2\cdot T_{amb} + T_{PCB} + T_{cc}\right) \tag{1}$$

- Thermal expansion mismatch (τ_c): This equation provides a measure of engineering strain. This equation utilizes the following variables: the printed circuit board coefficient of thermal expansion (α_{PCB}), the chip carrier coefficient of thermal expansion (α_{cc}), T_{PCB}, T_{amb}, and T_{cc}.

$$\tau_c := \alpha_{PCB}\cdot\left(T_{PCB} - T_{amb}\right) + \alpha_{cc}\cdot\left(T_{cc} - T_{amb}\right) \tag{2}$$

- Shear Strain in Solder (γ_c): This equation describes the shear strain experienced by the solder as a result of the thermal expansion mismatch. This equation utilizes the following variables: the solder height (H), the non-ideality coefficient (C), the characteristic length (L_o), and τ_c.

$$\gamma_c := C\cdot\frac{L_o}{H}\cdot\tau_c \tag{3}$$

- Mason-Coffin fatigue life equation (N_f): This equation allows the determination of cycles the solder will survive prior to failing, using γ_c. From experimental data for a given mean solder temperature and number of cycles per hour, the fatigue ductility coefficient d and fatigue ductility exponent e can be determined.

$$N_f := \left(\frac{1}{2}\right)\cdot\left(\frac{\gamma_c}{d}\right)^{\left(\frac{1}{e}\right)} \tag{4}$$

- Thermal strain (ε_{TS}): This equation tells the strain undergone in the solder due to the temperature change, through the use of the young modulus of the solder (E_s) and the thermal stress (σ_{TS}).

$$\sigma_{TS} := E_S \cdot \varepsilon_{TS} \tag{5}$$

- Thermal stress (σ_{TS}): This equation tells the thermal stress based on Hooke's law and the previously calculated thermal strain.

$$\sigma_{TS} := E_S \cdot \varepsilon_{TS} \tag{6}$$

- Factor of safety (FS): This equation compares the experienced stresses (σ_{TS}) with the yield strength of the material (σ_{yS}).

$$FS := \frac{\sigma_{yS}}{\sigma_{TS}} \tag{7}$$

Table 2 displays the analytical results that were obtained after using the aforementioned equations:

Table 2. Analytical results.

Parameter	**Result**
Mean solder temp	23.624 °C
Thermal expansion mismatch	6.261×10^{-4}
Shear strain	0.02546
Thermal strain in solder	1.937×10^{-4}
Thermal stress in solder	1.937 MPa
Thermal mismatch stress in solder	6.261 MPa
Factor of safety for solder thermal stress	18.07
Factor of safety for solder von Mises stress	24.38
Factor of safety for solder thermal mismatch stress	5.59
Number of cycles to failure	3024 cycles

The thermal strain in the solder as a function of time can be seen in Figure 24. The strain takes approximately 300 seconds before it reaches the steady state analysis value. Figure 24 also shows a correlation between calculated strain and the strain extracted from COMSOL. The results match near perfectly.

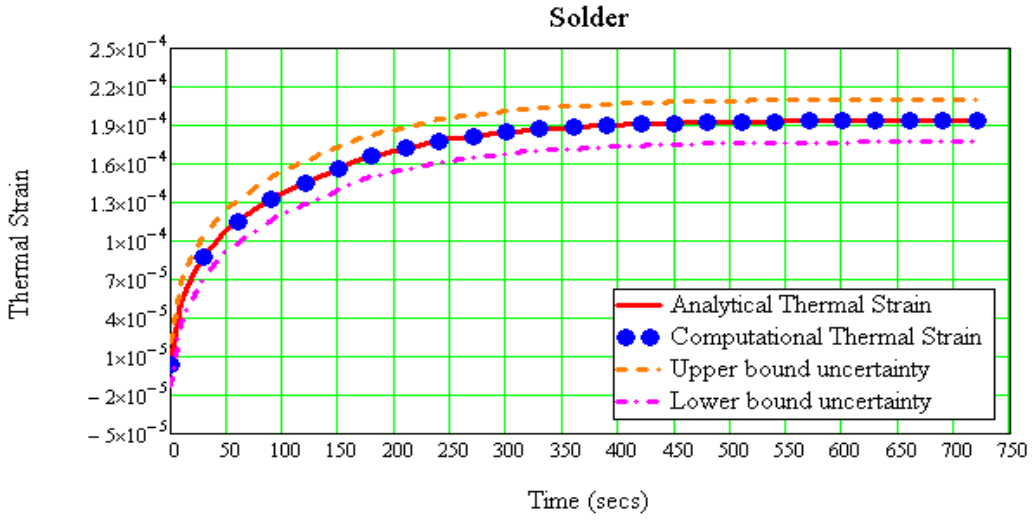

Figure 24. Solder: thermal strain vs. time.

Figure 25 shows the resulting thermal stress and the comparison with the von Mises stress extracted from COMSOL. It can be seen that the thermal stress is higher than the von Mises by about 0.5MPa. This can be attributed to the fact that the von Mises stress data was an average of the solder volume as discussed above. However, the results still fall within an order of magnitude of one another.

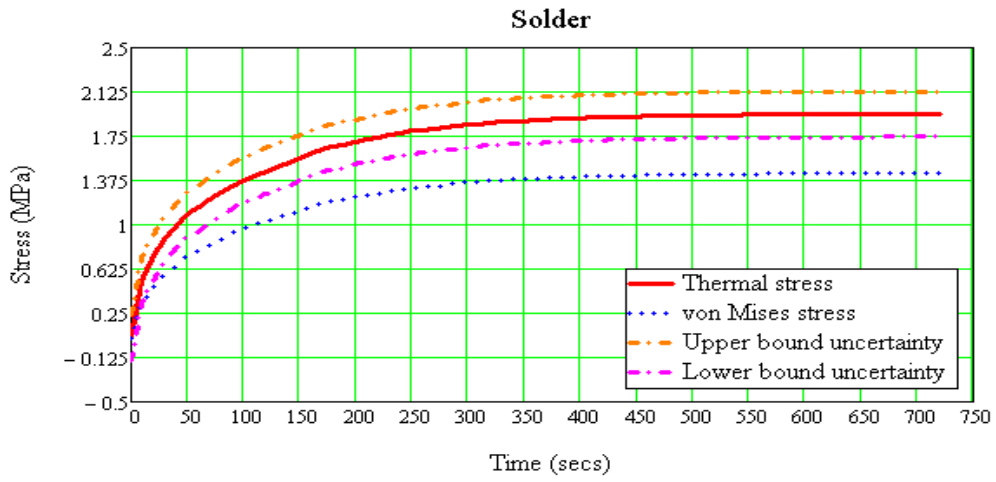

Figure 25. Solder: stress vs. time.

Figure 26 represents of the factor of safety for these two stresses. With this plot we are able to observe that the factor of safety for this component, over the applied load, is quite high. Thus, the component will not fail under ordinary operating conditions.

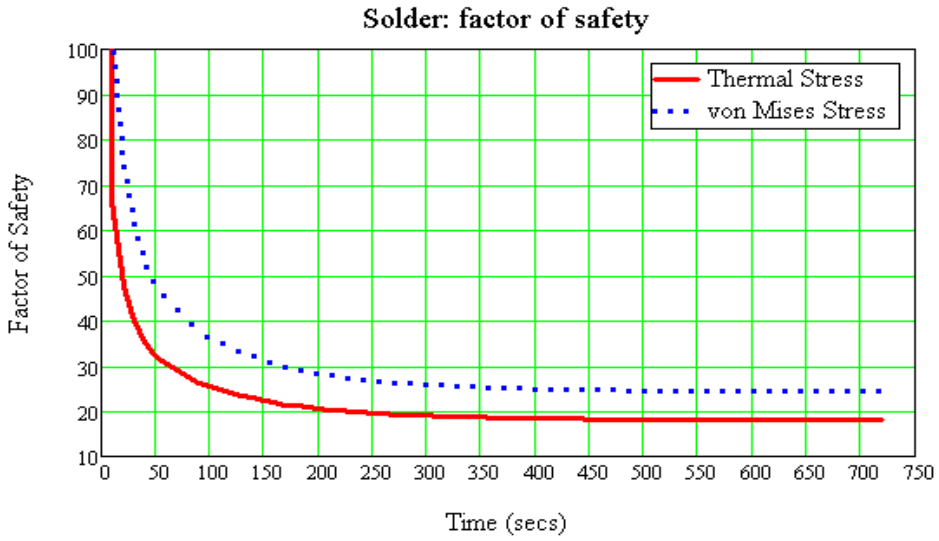

Figure 26. Solder: factor of safety vs. time.

12.2.2. Connections to uncertainty analysis

The uncertainty analysis provided vital insight into the component's performance. Utilizing the RSS uncertainty equation (8), the overall uncertainty for the number of cycles to failure (δNf) can be calculated (Pryputniewicz, 2013). To determine this uncertainty, the following uncertainties were needed: the fatigue ductility coefficient contribution to uncertainty in number of cycles to failure (δNfδd), the fatigue ductility exponent contribution to uncertainty in number of cycles to failure (δNfδe), and the shear strain contribution to uncertainty in number of cycles to failure (δNfδγ). Through careful iterations and trials the value of the uncertainty for the number of cycles for both the experimental model and the FEA analysis was reduced to around 5%. However, to achieve such a low percent of uncertainty there were several assumptions made on the uncertainties of the parameters governing this calculation.

$$\delta Nf := \left[(\delta Nf \delta \gamma)^2 + (\delta Nf \delta d)^2 + (\delta Nf \delta e)^2 \right]^{\frac{1}{2}} \tag{8}$$

The first trial assumed a 10% uncertainty for the each of the parameters used in the calculation. The calculations can be found in Appendix E. These assumed uncertainties were rather high, but this first trial served as a means to gain a better understanding of the percent contributions from each of the parameters to the overall uncertainty. The percent uncertainty for the FEA analysis was found to be 135.9% and the percent uncertainty for the experimental data was 141.5%. Clearly these values are above the expected uncertainty limits and require modifications to drive the uncertainty down.

The second trial allowed the overall percent uncertainty in the number of cycles to failure to be reduced to 5%. The values in Table 3 were selected as the ones required for obtaining the desired percent uncertainty. These values were selected under ideal assumptions of the near exact knowledge of the parameters used in the calculation. The majority of these were around 1%. For the non-ideality constant C, the ductility fatigue coefficient, and the ductility fatigue exponent, an assumption of one half the least significant digit was made. It is understood that for the non-ideality coefficient, the original uncertainty was 0.25, or the difference between the average of the limits of this coefficient and each of the extrema. For sake of obtaining the 5% uncertainty, however, the previous assumption was made.

Table 3. Selected uncertainties for analysis.

Variable	**Units**	**Value**	**Uncertainty**
αs	1/K	1.80×10^{-5}	1.8×10^{-7}
αcc	1/K	5.85×10^{-5}	5.85×10^{-7}
Lo	mm	3.163	0.032
H	mm	0.105	1.05×10^{-3}
d		0.7739	0.00005
e		-0.3921	0.00005
C		1.35	0.005
COMSOL values			
To	K	293.15	0.1
Ts	K	298.63	0.255
Tcc	K	302.17	0.029
Experimental values			
To	*C	20.5	0.103
Ts	*C	27.5	0.28
Tcc	*C	28	0.028

The information from the uncertainty analysis coupled with the experimental and the FEA results can paint a vivid picture of the behavior of an SMT component. With these results, an evaluation model for further analysis of surface mount components, thermo-mechanical behavior is proposed. The combination of analytical, computational, and experimental results yields a well-rounded solution of the intricate behavior of microelectronics. Furthermore, each of the results helps validate each of the solutions obtained.

13. Conclusions and recommendations

Through the comparison of the computational modeling and analytical (graphical) results, we were able to show consistent findings across the different solution methods. Both the analytical and computational values were shown to fall within the limits of the measured uncertainty values. For each measured value we observed a monotonic progression, indicating the absence of fluctuation in these values over time. The correlation between the results of the different solution methods validates the ability to accurately model components and the conditions that they experience in functional applications.

In planning and implementing the methodologies involved in this MQP our group was able to accomplish a large portion of our goals; however, looking back on the project we realize that there are several things we could have done that would have made for smoother implementation and more accurate results. One factor that played a major role in our project was time. Initially our project was scheduled to run A, B, and C-Term of the 2012-2013 school year, but, in order to produce more complete results our group decided to extend the project into D-Term of 2013. Had we known that our project would be going throughout the whole school year we may have been able to conduct further analyses of our sample PCBs. Another factor that added further limitations to our project was devoting a lot of time contacting with SMT manufacturers and industry leaders in hopes of gaining feedback and assistance from them. We believed that through doing this we would be able to receive insight and wisdom from these companies, sample PCBs, and perhaps facilities to conduct our experiments. Unfortunately, this was not the case. We received very little feedback from the companies that we reached out to and

due to the amount of time put into contacting them, we gave ourselves further, unnecessary time constraints.

Looking back, if we were to begin the project again we would still attempt to contact various companies, but we wouldn't count as heavily on a response, we would work with the PCBs we had, in the facilities available to us in order to guarantee the forward progress of the project. In addition to this, our group would have modeled the full PCB that we had, rather than just one SMD. Again, due to some of the time constraints of the project, in addition to the learning curve of the software we used, contributed to this, but ideally the full PCB would have been modeled as it would be a more accurate representation of the actual PCB. With our given boundary conditions, we were able to produce accurate models and analyses of the single SMD, but being able to model and analyze the whole board and observe how each of the SMDs interact with each other, as well as the PCB, would have been beneficial. Going back, we would have liked to explore more of the effects of power cycling and vibrations on solder, but again, the equipment and time available to us didn't allow for it. Additionally, if we were given more time we would have liked to utilize the lasers and optics labs on the WPI campus to conduct more actual experimentation but with the learning curve involved with the equipment it was just not possible to fit it all in. Based on both our prior research and work on this project, our recommendation for future projects researching this subject matter would be to place more focus on the material properties of solder and the optimization of solder for electronic components in general.

14. References

Actel. (2003, June). Assembly Instructions for CQFP Packages SMT on PCB. Sunnyvale, California.

Analog Devices. "Single Supply, Rail-to-Rail, Low Cost Instrumentation Amplifier," Norwood, MA. (2008). AD623 Chip. Last Accessed: 23 April 2013. Available from http://www.analog.com

Ashby, M. and Cebon, D., CES Granta Edupack (Version 11.9.9) [Computer Software]. Cambridge, UK. Last accessed: 25 March 2013. Available from http://www.grantadesign.com/

Blattau, D. N. (2012, February 23). Exploring Vibration Fatigue of Electronic Assemblies. College Park, Maryland.

Dassault Systèmes SolidWorks Corporation, SolidWorks Education Edition (2011-2012) [Computer Software]. Waltham, MA. Last accessed: 22 April 2013. Available from http://www.solidworks.com

EIA, "Environmental Test Methodology for Assessing the Performance of Electrical Connectors and Sockets Used in Business Office Applications (EIA-364-1000)," Electronic Industries Alliance 2001, Arlington, VA. (2000, December) Last Accessed: 23 April 2013. Available from http://www.ec-central.org.

Ghaffarian, D. R. (1995). SMT Solder Joint Reliability/Workmanship Environmental Test Results Correlation for LCC Assemblies. Pasadena, California, United States.

Hedge, P., Whalley, D.C. and Silberschmidt, V.V., 2008. Thermo-mechanical damage accumulation during power cycling of lead-free surface mount solder joints. IN: Proceedings, 2nd IEEE Electronics Systemintegration Technology Conference, Greenwich, 1-4 Sept. 2008, pp. 1081 - 1090

Hines, J., Stanczak, A., Decker, D., and Kanjanupathum, T. (2011). *Solder Charge Grid Array: Advancements In The Technology Of Surface Mount Area Array Solder Joint Attachment.* Lisle, IL: Molex Inc.

Incropera, F. P., DeWitt, D. P. (2007). *Fundamentals of Heat and Mass Transfer*, 6th ed., Wiley, New York, p. 8.

Intel, Ch. 2, “Package/Module/PC Card outlines and dimensions,” *Intel packaging databook*, http://www.intel.com/content/dam/www/public/us/en/documents/packaging-databooks/packaging-chapter-02-databook.pdf (last accessed: 25 March 2013)

Intel, Ch. 5, “Constants of IC package,” *Intel packaging databook*, http://www.intel.com/content/dam/www/public/us/en/documents/packaging-databooks/packaging-chapter-05-databook.pdf (last accessed: 25 March 2013)

IPC, "Performance Test Methods and Qualification Requirements for Surface Mount Solder Attachments (IPC-9701)," Bannockburn, IL. (2002, January) Last Accessed: 23 April 2013. Available from http://www.ipc.org.

Koebrich, J., *Watchfire Signs,* Danville, IL, personal communication, 2012.

Kühl, Reiner W. (1999),"Mechanical stress and deformation of SMT components during temperature cycling and PCB bending", Soldering & Surface Mount Technology, Vol. 11 Iss: 2 pp. 35 – 41.

Littmarck, S. and Saeidi, F., COMSOL multiphysics (Version 4.3a) [Computer Software]. Burlington, MA. Last accessed: 25 March 2013. Available from http://www.comsol.com/

Pryputniewicz, R., and Stupnicki, J. (1994, Novemeber 30). Hybrid approach to deformation analysis. *Interferometry '94: Photomechanics, Ed.*, 282-296.

Pryputniewicz, R.J., (2013). *Integrated Thermomechanical Design and Analysis with Applications to Micromechatronics*, ME/CHSLT-NEST, Worcester Polytechnic Institute, Department of Mechanical Engineering. Worcester Polytechnic Institute, Worcester, MA, p. 122-159

Pryputniewicz, R.J., Rosato, D., and Furlong, C., "Noninvasive measurements and computational modeling of SMT assemblies," *Paper No. IMECE2001/EPP-24713*, ASME - Am Soc. Mech. Eng., New York, NY, 2001

Pryputniewicz, R.J., Rosato, D., and Furlong, C., "Measurements and simulation of SMT components," *Proc. 35th Internat. Symp. on Microelectronics*, Denver, CO, pp. 151-156, 2002

Pryputniewicz, D.R., Furlong, C., and Pryputniewicz, R.J., "SMT: modeling and uncertainty analysis of a J-lead attachment," *Proc. 35th Internat. Symp. on Microelectronics*, Denver, CO, pp. 157-162, 2002

Pryputniewicz, R.J., Rosato, D., and Furlong, C., "Measurements and simulation of SMT components," *Microelectronics Internat*., 20:13-16, 2003.

Tu, P. L., Chan, Y. C., Lai, J. K. (1997, February). Effect of Intermetallic Compounds on the Thermal Fatigue of Surface Mount Solder Joints. *IEEE Transactions on Components, Packaging, and Manufacturing Technology, 20*(1), pp. 87-93.

Xiao, Yu, *BGRIMM*, Beijing, personal communication, 2013.

15. Appendices

15.1. Appendix A – Part-specific materials

Case materials:

Properties	Units	Alumina (92%)	Kovar	Molding Compound	Sealing Glass	Cu-W (90%)	Cu
Density	kg/m^3 (g/cc)	3600-3700 (3.6-3.7)	8400 (8.4)	1790-1850 (1.79-1.85)	4700 (4.7)	17000 (17)	8900 (8.9)
Modulus of Elasticity	GPa	55	138	E_1 = 11.7 E_2 = 0.1	5.7	255	125
Tensile Strength	MPa	157	627	19.98			270
Thermal Conductivity (20°C)	W/mK	18	17.5	0.58 -0.67	0.6	180 - 200	
Coefficient of Thermal Expansion	ppm/°C	6.8 (25°C - 400°C)	5.3 (40°C - 250°C)	$a_1 \leq 23$ $a_2 \leq 80$ (40°C - 250°C)	6.3 - 7.0 (40°C - 250°C)	6.5 (25°C - 500°C)	16 (25°C - 500°C)
Electrical Resistivity	Ω cm	10^{14}	49 X 10^{-6}	5 X 10^{12}	$>10^{11}$	<6 X 10^{-6}	<2 X 16^{-6}
Dielectric Constant (1 MHz)		7.9 - 10.0	NA	$\leq$ 5.0	11.5	NA	NA

Lead/Lead Frame materials:

Properties	Units	Copper Alloy MF 202	Alloy 42	Kovar	TAMAC5	CDA 194	OLIN 7025	EFTEC 64T
Density	kg/m^3 (g/cc)	8880 (8.8)	8100 (8.1)	8400 (8.4)	8900 (8.9)	8800 (8.8)	8800 (8.8)	8900 (8.9)
Modulus of Elasticity	GPa	113	145	138	120	121	131	119
Tensile Strength	MPa	490-590	588-735	627	527-562	480-519	527	560
Thermal Conductivity (20°C)	W/mK	160	15.7	17.5	138	263	166	300
Coefficient of Thermal Expansion	ppm/°C	17.0	4.5	5.3	16.7	16.3	17.1	17.0
Electrical Resistivity	Ω cm	5.7 X 10^{-6}	57 X 10^{-6}	49 X 10^{-6}	4.9 X 10^{-6}	2.6 X 10^{-6}	4.3 X 10^{-6}	2.3 X 10^{-6}

Solder materials and melting temperatures:

Solder Type	Temperature (°C)
Sn-Pb Plating (85 wt% Sn)	200 - 225
Sn-Pb Eutectic (62 wt% Sn)	183
Tin	232
Lead	327
Gold	1063
Copper	1083
Silver	961
Copper/Silver Braze (28 wt% Cu)	850
Au-Sn Eutectic (80 wt% Au)	280

Die attach materials:

Property	Units	Silver Filled Glass	Silver Filled Adhesive	Silver Filled Epoxy	99.99% Au + 2% Si	99.99% Au
Density	kg/m^3 (g/cc)	4500 (4.5)		2500 (2.5)	14500 (14.5)	19300 (19.3)
Modulus Elasticity	GPa		0.77		69.5 (Data for Au + 3% Si)	62.5
Tensile Strength	MPa	> 10.			500-600	130
Thermal Conductivity	W/mK	270	2.5 @ 121°C	1.6 @ 121°C	50	311
Coefficient of Thermal Expansion	ppm/°C	8	$\alpha_1 = 40$ $\alpha_2 = 150$	$\alpha_1 = 46$ $\alpha_2 = 240$	50 @ 25°C	14.2 @ 25°C
Electrical Resistivity	Ω cm	1×10^{-5}	1×10^{-4}	2×10^{-4}	3.1×10^{-4}	2.21×10^{-6}

15.2. Appendix B – Manufacturer questionnaire

Company Questionnaire

Roberto Alvarado, Michael Bartlett, Richard Beski, Santiago Isaza, Congji Li
A Term ’12 – C Term ‘13
October 19, 2012

Submitted to:
Prof. R. J. Pryputniewicz
WPI-ME/CHSLT-NEST

When designing a product that implements Surface Mounted Technology (SMT), what are some of the considerations your company takes into account? For example, do you focus on potential failures first or do you try to design a product and deal with issues as they come up?

What are some of the frequent failures your company deals with?

What standards do you employ when designing a new product? Do you follow an established set of standards like the IPC-A-610E or do you have your own set of standards? If so, what are they?

What is your quality control testing like? How long is the process and how often do you catch issues because of it? Again, does your company use standards like the IPC-9701A or does it utilize its own standards?

Do you get any reports of failures from consumers? If so, how often are they? Can you comment on how these issues are mitigated?

What future do you see for SMTs? Where does your company want to take SMTs in the future?

Could you please suggest any other issues/developments pertaining to the current state of the art in SMT?

15.3. Appendix C – Material tables

The materials selected and their properties are as followed:

Printed circuit board:
FR4

Property	Value	Unit
Electrical conductivity	0.004	S/m
Relative permittivity	4.5	1
Coefficient of thermal expansion	1.80E-05	1/K
Heat capacity at constant pressure	1369	J/kg-K
Density	1900	kg/m^3
Thermal conductivity	0.3	W/m-K
Young's modulus	2.20E+10	Pa
Poisson's ratio	0.28	1
Relative permeability	1	1
Yield Strength	1.19E+8	Pa

Chip carrier case:
Acrylic Plastic

Property	Value	Unit
Electrical conductivity	3.33E-17	S/m
Relative permittivity	3.3	1
Coefficient of thermal expansion	7.0E-05	1/K
Heat capacity at constant pressure	1470	J/kg-K
Density	1190	kg/m^3
Thermal conductivity	0.18	W/m-K
Young's modulus	3.2E+9	Pa
Poisson's ratio	0.35	1
Yield Strength	6.31E+7	Pa

Alumina (Al2O3)

Property	Value	Unit
Electrical conductivity	1E-13	S/m
Relative permittivity	3.9.6	1
Coefficient of thermal expansion	6.5E-06	1/K
Heat capacity at constant pressure	730	J/kg-K
Density	3965	kg/m^3
Thermal conductivity	35	W/m-K
Young's modulus	400E+9	Pa
Poisson's ratio	0.22	1
Yield Strength	2.63E+8	Pa

PMMA

Property	Value	Unit
Electrical conductivity	1E-14	S/m
Relative permittivity	3.3	1
Coefficient of thermal expansion	7.0E-05	1/K
Heat capacity at constant pressure	1420	J/kg-K
Density	1190	kg/m^3
Thermal conductivity	0.19	W/m-K
Young's modulus	3E+9	Pa
Poisson's ratio	0.40	1
Yield Strength	4.47E+7	Pa

Polyimide

Property	Value	Unit
Electrical conductivity	3.71E-14	S/m
Relative permittivity	4	1
Coefficient of thermal expansion	5.85E-05	1/K
Heat capacity at constant pressure	1100	J/kg-K
Density	1300	kg/m^3
Thermal conductivity	0.15	W/m-K
Young's modulus	3.1E+9	Pa
Poisson's ratio	0.34	1
Yield Strength	1.15E+8	Pa

Lead/Lead-frame/PCB wire:
Copper (Cu)

Property	Value	Unit
Electrical conductivity	5.998E+7	S/m
Relative permittivity	1	1
Coefficient of thermal expansion	1.66E-04	1/K
Heat capacity at constant pressure	385	J/kg-K
Density	8700	kg/m^3
Thermal conductivity	400	W/m-K
Young's modulus	1.17E+11	Pa
Poisson's ratio	0.36	1
Yield Strength	5.0E+7	Pa

Aluminum (Al)

Property	Value	Unit
Electrical conductivity	3.35E+6	S/m
Relative permittivity	1	1
Coefficient of thermal expansion	23.1E-06	1/K
Heat capacity at constant pressure	904	J/kg-K
Density	2700	kg/m^3
Thermal conductivity	237	W/m-K
Young's modulus	70E+9	Pa
Poisson's ratio	0.35	1
Yield Strength	3.0E+7	Pa

Solder:
60Sn-40Pb

Property	Value	Unit
Electrical conductivity	6.67E+6	S/m
Relative permittivity	.99	1
Coefficient of thermal expansion	21E-06	1/K
Heat capacity at constant pressure	150	J/kg-K
Density	9000	kg/m^3
Thermal conductivity	50	W/m-K
Young's modulus	10E+9	Pa
Poisson's ratio	0.40	1
Yield Strength	3.5E+7	Pa

Die attach:
Ag filled epoxy (85wt% Ag) [fully cured at 423K]

Property	Value	Unit
Electrical conductivity	5.0E+6	S/m
Relative permittivity	1.3	1
Coefficient of thermal expansion	9.51E-05	1/K
Heat capacity at constant pressure	380.6	J/kg-K
Density	2500	kg/m^3
Thermal conductivity	8.8	W/m-K
Young's modulus	70E+9	Pa
Poisson's ratio	0.35	1
Yield Strength (estimated)	2.3E+8	Pa

Chip:
Si(c)

Property	Value	Unit
Electrical conductivity	3.12E-8	S/m
Relative permittivity	11.7	1
Coefficient of thermal expansion	2.6E-06	1/K
Heat capacity at constant pressure	700	J/kg-K
Density	2329	kg/m^3
Thermal conductivity	130	W/m-K
Young's modulus	170E+9	Pa
Poisson's ratio	0.28	1
Yield Strength	1.72E+8	Pa

15.4. Appendix D – AD623 datasheet

Excerpts from full datasheet have been included based on what has been used:

ANALOG DEVICES

Single-Supply, Rail-to-Rail, Low Cost Instrumentation Amplifier

AD623

FEATURES

Easy to use
Higher performance than discrete design
Single-supply and dual-supply operation
Rail-to-rail output swing
Input voltage range extends 150 mV below ground (single supply)
Low power, 550 µA maximum supply current
Gain set with one external resistor
Gain range: 1 (no resistor) to 1000
High accuracy dc performance
0.10% gain accuracy (G = 1)
0.35% gain accuracy (G > 1)
10 ppm maximum gain drift (G = 1)
200 µV maximum input offset voltage (AD623A)
2 µV/°C maximum input offset drift (AD623A)
100 µV maximum input offset voltage (AD623B)
1 µV/°C maximum input offset drift (AD623B)
25 nA maximum input bias current
Noise: 35 nV/√Hz RTI noise @ 1 kHz (G = 1)
Excellent ac specifications
90 dB minimum CMRR (G = 10); 70 dB minimum CMRR (G = 1) at 60 Hz, 1 kΩ source imbalance
800 kHz bandwidth (G = 1)
20 µs settling time to 0.01% (G = 10)

APPLICATIONS

Low power medical instrumentation
Transducer interfaces
Thermocouple amplifiers
Industrial process controls
Difference amplifiers
Low power data acquisition

GENERAL DESCRIPTION

The AD623 is an integrated single-supply instrumentation amplifier that delivers rail-to-rail output swing on a 3 V to 12 V supply. The AD623 offers superior user flexibility by allowing single gain set resistor programming and by conforming to the 8-lead industry standard pinout configuration. With no external resistor, the AD623 is configured for unity gain (G = 1), and with an external resistor, the AD623 can be programmed for gains up to 1000.

CONNECTION DIAGRAM

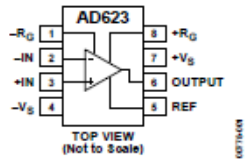

Figure 1. 8-Lead PDIP (N), SOIC (R), and MSOP (RM) Packages

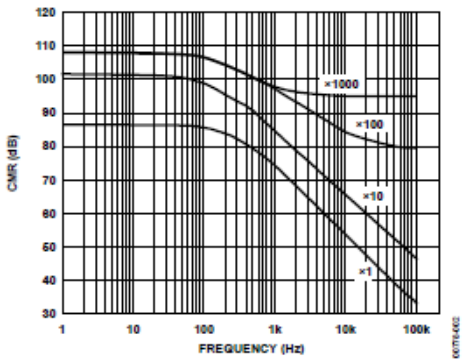

Figure 2. CMR vs. Frequency, 5 V_S, 0 V_S

The AD623 holds errors to a minimum by providing superior ac CMRR that increases with increasing gain. Line noise, as well as line harmonics, are rejected because the CMRR remains constant up to 200 Hz. The AD623 has a wide input common-mode range and can amplify signals that have a common-mode voltage 150 mV below ground. Although the design of the AD623 was optimized to operate from a single supply, the AD623 still provides superior performance when operated from a dual voltage supply (±2.5 V to ±6.0 V).

Low power consumption (1.5 mW at 3 V), wide supply voltage range, and rail-to-rail output swing make the AD623 ideal for battery-powered applications. The rail-to-rail output stage maximizes the dynamic range when operating from low supply voltages. The AD623 replaces discrete instrumentation amplifier designs and offers superior linearity, temperature stability, and reliability in a minimum of space.

OUTLINE DIMENSIONS

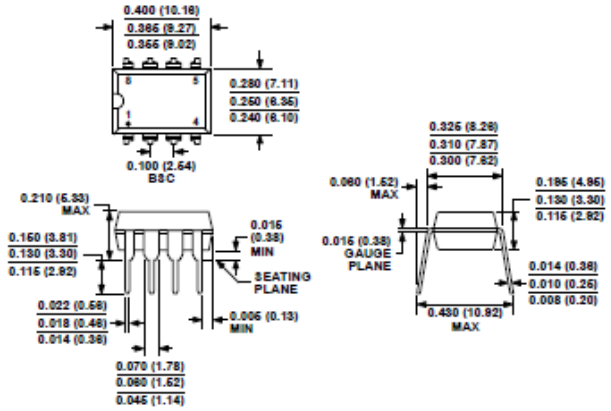

COMPLIANT TO JEDEC STANDARDS MS-001

CONTROLLING DIMENSIONS ARE IN INCHES; MILLIMETER DIMENSIONS (IN PARENTHESES) ARE ROUNDED-OFF INCH EQUIVALENTS FOR REFERENCE ONLY AND ARE NOT APPROPRIATE FOR USE IN DESIGN. CORNER LEADS MAY BE CONFIGURED AS WHOLE OR HALF LEADS.

Figure 56. 8-Lead Plastic Dual In-Line Package [PDIP]
Narrow Body (N-8)
Dimensions shown in inches and (millimeters)

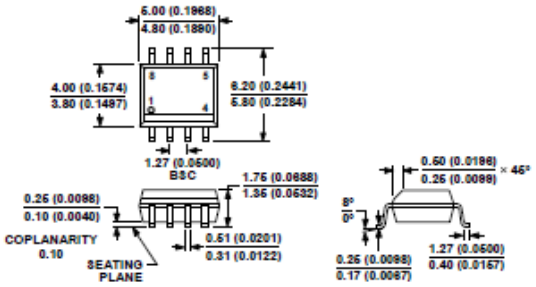

COMPLIANT TO JEDEC STANDARDS MS-012-AA

CONTROLLING DIMENSIONS ARE IN MILLIMETERS; INCH DIMENSIONS (IN PARENTHESES) ARE ROUNDED-OFF MILLIMETER EQUIVALENTS FOR REFERENCE ONLY AND ARE NOT APPROPRIATE FOR USE IN DESIGN.

Figure 57. 8-Lead Standard Small Outline Package [SOIC_N]
Narrow Body (R-8)
Dimensions shown in millimeters and (inches)

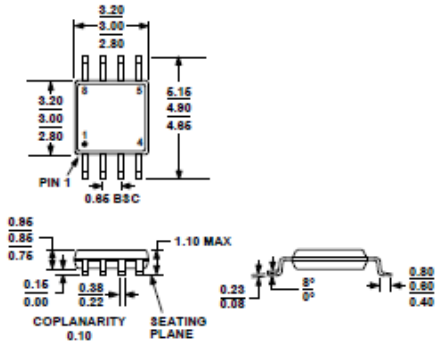

Figure 58. 8-Lead Mini Small Outline Package [MSOP]
(RM-8)
Dimensions shown in millimeters

ORDERING GUIDE

Model	Temperature Range	Package Description	Package Option	Branding
AD623AN	−40°C to +85°C	8-Lead Plastic Dual In-Line Package [PDIP]	N-8	
AD623ANZ[1]	−40°C to +85°C	8-Lead Plastic Dual In-Line Package [PDIP]	N-8	
AD623AR	−40°C to +85°C	8-Lead Standard Small Outline Package [SOIC_N]	R-8	
AD623AR-REEL	−40°C to +85°C	8-Lead Standard Small Outline Package [SOIC_N], 13" Tape and Reel	R-8	
AD623AR-REEL7	−40°C to +85°C	8-Lead Standard Small Outline Package [SOIC_N], 7" Tape and Reel	R-8	
AD623ARZ[1]	−40°C to +85°C	8-Lead Standard Small Outline Package [SOIC_N]	R-8	
AD623ARZ-R7[1]	−40°C to +85°C	8-Lead Standard Small Outline Package [SOIC_N], 7" Tape and Reel	R-8	
AD623ARZ-RL[1]	−40°C to +85°C	8-Lead SOIC, 13" Tape and Reel	R-8	
AD623ARM	−40°C to +85°C	8-Lead Mini Small Outline Package [MSOP]	RM-8	J0A
AD623ARM-REEL	−40°C to +85°C	8-Lead Mini Small Outline Package [MSOP], 13" Tape and Reel	RM-8	J0A
AD623ARM-REEL7	−40°C to +85°C	8-Lead Mini Small Outline Package [MSOP], 7" Tape and Reel	RM-8	J0A
AD623ARMZ[1]	−40°C to +85°C	8-Lead Mini Small Outline Package [MSOP]	RM-8	J0A
AD623ARMZ-REEL[1]	−40°C to +85°C	8-Lead Mini Small Outline Package [MSOP], 13" Tape and Reel	RM-8	J0A
AD623ARMZ-REEL7[1]	−40°C to +85°C	8-Lead Mini Small Outline Package [MSOP], 7" Tape and Reel	RM-8	J0A
AD623BN	−40°C to +85°C	8-Lead Plastic Dual In-Line Package [PDIP]	N-8	
AD623BNZ[1]	−40°C to +85°C	8-Lead Plastic Dual In-Line Package [PDIP]	N-8	
AD623BR	−40°C to +85°C	8-Lead Standard Small Outline Package [SOIC_N]	R-8	
AD623BR-REEL	−40°C to +85°C	8-Lead Standard Small Outline Package [SOIC_N], 13" Tape and Reel	R-8	
AD623BR-REEL7	−40°C to +85°C	8-Lead Standard Small Outline Package [SOIC_N], 7" Tape and Reel	R-8	
AD623BRZ[1]	−40°C to +85°C	8-Lead Standard Small Outline Package [SOIC_N]	R-8	
AD623BRZ-R7[1]	−40°C to +85°C	8-Lead Standard Small Outline Package [SOIC_N], 7" Tape and Reel	R-8	
AD623BRZ-RL[1]	−40°C to +85°C	8-Lead Standard Small Outline Package [SOIC_N], 13" Tape and Reel	R-8	
EVAL-INAMP-62RZ[1]		Evaluation Board		

[1] Z = RoHS Compliant Part.

15.5. Appendix E – MathCad calculations

Values obtaind from COMSOL analysis:

$T_{PCB} := 298.630700632362$ K

$T_{amb} := 293.15$ K

$T_{cc} := 302.166691799585$ K

$T_S := 302.375154446617$ K

$\epsilon_S := 0.00054962359812317$

$\sigma_S := 1.43561436238536$ MPa

Experimental Results:

Tpcb := 27.5 °C Tamb := 20.5 °C

Tcc := 28 °C

Material properties and characteristic parameters:

$\alpha_{PCB} := 1.80 \cdot 10^{-5}$ 1/K

$\alpha_S := 21 \cdot 10^{-6}$ 1/K

$\alpha_{cc} := 5.85 \cdot 10^{-5}$ 1/K

$E_S := 10 \cdot 10^3$ MPa

$\sigma_{yPCB} := 1.19 \cdot 10^2$ MPa

$\sigma_{yS} := 35$ MPa

$\sigma_{ycc} := 1.15 \cdot 10^2$ MPa

$l_{cc} := 2.45$ mm

$w_{cc} := 2$ mm

$L_o := \sqrt{l_{cc}^2 + w_{cc}^2}$

$L_o = 3.163$ mm

$H := 0.105$ mm

$C := 1.35$

Assuming:
Tsm:=298.15K
cph:= 4

$d := 0.7739$

$e := -0.3921$

Uncertainties:

$\delta\alpha_s := 10\% \cdot \alpha_{PCB} = 1.8 \times 10^{-6}$ 1/K

$\delta\alpha_{cc} := 10\% \cdot \alpha_{cc} = 5.85 \times 10^{-6}$ 1/K

$\delta L := 10\% \cdot L_o = 0.316$ mm

$\delta H := 10\% \cdot H = 0.011$ mm

$\delta d := d \cdot 10\% = 0.07739$

$\delta e := e \cdot 10\% = -0.039$

$\delta c := 0.25$

Comsol values:

$\delta T_o := (T_{amb} - 273.15) \cdot 10\% = 2$ K

$\delta T_s := (T_{PCB} - 273.15) \cdot 10\% = 2.548$ K

$\delta T_{cc} := (T_{cc} - 273.15) \cdot 10\% = 2.902$ K

Experimental values:

δTo := (Tamb)·10% = 2.05 °C

δTs := (Tpcb)·10% = 2.75 °C

δTcc := (Tcc)·10% = 2.8 °C

Analysis :

Comsol values:

$T_{sm} := \frac{1}{4}\cdot(2\cdot T_{amb} + T_{PCB} + T_{cc})$ $T_{sm} = 296.774$ *C

$\%conv := \frac{T_{sm} - 298.15}{T_{sm}}\cdot 100$ $\%conv = -0.464$ %

$\tau_c := \alpha_{PCB}\cdot(T_{PCB} - T_{amb}) + \alpha_{cc}\cdot(T_{cc} - T_{amb})$ $\tau_c = 6.261 \times 10^{-4}$

$\gamma_c := C\cdot\frac{L_o}{H}\cdot\tau_c$ $\gamma_c = 0.02546$

$N_f := \left(\frac{1}{2}\right)\cdot\left(\frac{\gamma_c}{d}\right)^{\left(\frac{1}{e}\right)}$ $N_f = 3024.928$ cycles

Experimental values:

$T_{sme} := \frac{1}{4}\cdot(2\cdot Tamb + Tpcb + Tcc)$ $T_{sme} = 24.125$ *C

$\%conve := \frac{T_{sme} - 298.15}{T_{sme}}\cdot 100$ $\%conve = -1.136 \times 10^{3}$ %

$\tau_{ce} := \alpha_{PCB}\cdot(Tpcb - Tamb) + \alpha_{cc}\cdot(Tcc - Tamb)$ $\tau_{ce} = 5.647 \times 10^{-4}$

$\gamma_{ce} := C\cdot\frac{L_o}{H}\cdot\tau_{ce}$ $\gamma_{ce} = 0.02296$

$N_{fe} := \left(\frac{1}{2}\right)\cdot\left(\frac{\gamma_{ce}}{d}\right)^{\left(\frac{1}{e}\right)}$ $N_{fe} = 3935.42$ cycles

$\varepsilon_{TS} := \alpha_S\cdot(T_S - T_{amb})$ $\varepsilon_{TS} = 1.937 \times 10^{-4}$

$\sigma_{TS} := E_S\cdot\varepsilon_{TS}$ $\sigma_{TS} = 1.937$ MPa

Solder von Mises stress $\sigma_S = 1.436$ MPa

$\sigma_{\tau S} := E_S\cdot\tau_c$ $\sigma_{\tau S} = 6.261$ MPa

$\sigma_{\tau Se} := E_S\cdot\tau_{ce}$ $\sigma_{\tau Se} = 5.647$ MPa

$FS(\sigma) := \frac{\sigma_{yS}}{\sigma}$

$FS(\sigma_{TS}) = 18.067$ $FS(\sigma_S) = 24.38$ $FS(\sigma_{\tau S}) = 5.59$ $FS(\sigma_{\tau Se}) = 6.197$

Trial #1 Uncertainty Analysis:

For Comsol Values:

Thermal Expansion Mismatch Phenomenological Equation:

$$\tau = \tau(\alpha_s, \alpha_{cc}, T_s, T_{cc}, T_o)$$

$$\tau(\alpha_s, \alpha_{cc}, T_s, T_{cc}, T_o) := \alpha_s \cdot (T_s - T_o) - \alpha_{cc} \cdot (T_{cc} - T_o)$$

$$\delta\tau\delta\alpha_s := \frac{\partial}{\partial \alpha_{PCB}} \tau(\alpha_{PCB}, \alpha_{cc}, T_{PCB}, T_{cc}, T_{amb}) \cdot \delta\alpha_s \qquad \delta\tau\delta\alpha_s = 9.865 \times 10^{-6}$$

$$\delta\tau\delta\alpha_{cc} := \frac{\partial}{\partial \alpha_{cc}} \tau(\alpha_{PCB}, \alpha_{cc}, T_{PCB}, T_{cc}, T_{amb}) \cdot \delta\alpha_{cc} \qquad \delta\tau\delta\alpha_{cc} = -5.275 \times 10^{-5}$$

$$\delta\tau\delta T_s := \frac{\partial}{\partial T_{PCB}} \tau(\alpha_{PCB}, \alpha_{cc}, T_{PCB}, T_{cc}, T_{amb}) \cdot \delta T_s \qquad \delta\tau\delta T_s = 4.587 \times 10^{-5}$$

$$\delta\tau\delta T_{cc} := \frac{\partial}{\partial T_{cc}} \tau(\alpha_{PCB}, \alpha_{cc}, T_{PCB}, T_{cc}, T_{amb}) \cdot \delta T_{cc} \qquad \delta\tau\delta T_{cc} = -1.697 \times 10^{-4}$$

$$\delta\tau\delta T_o := \frac{\partial}{\partial T_{amb}} \tau(\alpha_{PCB}, \alpha_{cc}, T_{PCB}, T_{cc}, T_{amb}) \cdot \delta T_o \qquad \delta\tau\delta T_o = 8.1 \times 10^{-5}$$

$$\delta\tau := \left[(\delta\tau\delta\alpha_s)^2 + (\delta\tau\delta\alpha_{cc})^2 + (\delta\tau\delta T_s)^2 + (\delta\tau\delta T_{cc})^2 + (\delta\tau\delta T_o)^2 \right]^{\frac{1}{2}} \qquad \delta\tau = 2.009 \times 10^{-4}$$

$$\%\delta\tau := \frac{\delta\tau}{\tau_c} \cdot 100 \qquad \%\delta\tau = 32.085 \ \%$$

$$\%\delta\tau\delta\alpha_s := \frac{\delta\tau\delta\alpha_s^{\,2}}{\delta\tau^2} \cdot 100 \qquad \%\delta\tau\delta\alpha_s = 0.241 \ \%$$

$$\%\delta\tau\delta\alpha_{cc} := \frac{\delta\tau\delta\alpha_{cc}^{\,2}}{\delta\tau^2} \cdot 100 \qquad \%\delta\tau\delta\alpha_{cc} = 6.894 \ \%$$

$$\%\delta\tau\delta T_s := \frac{\delta\tau\delta T_s^{\,2}}{\delta\tau^2} \cdot 100 \qquad \%\delta\tau\delta T_s = 5.212 \ \%$$

$$\%\delta\tau\delta T_{cc} := \frac{\delta\tau\delta T_{cc}^{\,2}}{\delta\tau^2} \cdot 100 \qquad \%\delta\tau\delta T_{cc} = 71.396 \ \%$$

$$\%\delta\tau\delta T_o := \frac{\delta\tau\delta T_o^{\,2}}{\delta\tau^2} \cdot 100 \qquad \%\delta\tau\delta T_o = 16.257 \ \%$$

$$\%\Sigma_{\delta\tau} := \%\delta\tau\delta\alpha_s + \%\delta\tau\delta\alpha_{cc} + \%\delta\tau\delta T_s + \%\delta\tau\delta T_{cc} + \%\delta\tau\delta T_o = 100 \ \%$$

Shear Strain Phenomenological Equation:

$\gamma = \gamma(c, L_o, H, \tau)$

$$\gamma(C, L_o, H, \tau) := C \cdot \frac{L_o}{H} \cdot \tau$$

$$\delta\gamma\delta c := \frac{\partial}{\partial C}\gamma(C, L_o, H, \tau_c) \cdot \delta c \qquad \delta\gamma\delta c = 4.715 \times 10^{-3}$$

$$\delta\gamma\delta L := \frac{\partial}{\partial L_o}\gamma(C, L_o, H, \tau_c) \cdot \delta L \qquad \delta\gamma\delta L = 2.546 \times 10^{-3}$$

$$\delta\gamma\delta H := \frac{\partial}{\partial H}\gamma(C, L_o, H, \tau_c) \cdot \delta H \qquad \delta\gamma\delta H = -2.546 \times 10^{-3}$$

$$\delta\gamma\delta\tau := \frac{\partial}{\partial \tau_c}\gamma(C, L_o, H, \tau_c) \cdot \delta\tau \qquad \delta\gamma\delta\tau = 8.169 \times 10^{-3}$$

$$\delta\gamma := \left[(\delta\gamma\delta c)^2 + (\delta\gamma\delta L)^2 + (\delta\gamma\delta H)^2 + (\delta\gamma\delta\tau)^2\right]^{\frac{1}{2}} \qquad \delta\gamma = 0.01$$

$$\%\delta\gamma := \frac{\delta\gamma}{\gamma_c} \cdot 100 \qquad \%\delta\gamma = 39.653 \ \%$$

$$\%\delta\gamma\delta c := \frac{\delta\gamma\delta c^2}{\delta\gamma^2} \cdot 100 \qquad \%\delta\gamma\delta c = 21.81 \ \%$$

$$\%\delta\gamma\delta L := \frac{\delta\gamma\delta L^2}{\delta\gamma^2} \cdot 100 \qquad \%\delta\gamma\delta L = 6.36 \ \%$$

$$\%\delta\gamma\delta H := \frac{\delta\gamma\delta H^2}{\delta\gamma^2} \cdot 100 \qquad \%\delta\gamma\delta H = 6.36 \ \%$$

$$\%\delta\gamma\delta\tau := \frac{\delta\gamma\delta\tau^2}{\delta\gamma^2} \cdot 100 \qquad \%\delta\gamma\delta\tau = 65.471 \ \%$$

$$\%\Sigma_{\delta\gamma} := \%\delta\gamma\delta c + \%\delta\gamma\delta L + \%\delta\gamma\delta H + \%\delta\gamma\delta\tau \qquad \%\Sigma_{\delta\gamma} = 100 \ \%$$

Number of Cycles to Failure Phenomenological Equation:

$N_f = Nf(\gamma, d, e)$

$$Nf(\gamma, d, e) := \frac{1}{2} \cdot \left(\frac{\gamma}{d}\right)^{\frac{1}{e}}$$

$$\delta Nf\delta\gamma := \frac{\partial}{\partial \gamma_c} Nf(\gamma_c, d, e) \cdot \delta\gamma \qquad \delta Nf\delta\gamma = -3.059 \times 10^{3}$$

$$\delta Nf\delta d := \frac{\partial}{\partial d} Nf(\gamma_c, d, e) \cdot \delta d \qquad \delta Nf\delta d = 771.468$$

$$\delta Nf\delta e := \frac{\partial}{\partial e} Nf(\gamma_c, d, e) \cdot \delta e \qquad \delta Nf\delta e = -2.634 \times 10^3$$

$$\delta Nf := \left[(\delta Nf\delta\gamma)^2 + (\delta Nf\delta d)^2 + (\delta Nf\delta e)^2 \right]^{\frac{1}{2}} \qquad \delta Nf = 4.11 \times 10^3$$

$$\%\delta Nf := \frac{\delta Nf}{N_f} \cdot 100 \qquad \%\delta Nf = 135.869 \quad \%$$

$$\%\delta Nf\delta\gamma := \frac{\delta Nf\delta\gamma^2}{\delta Nf^2} \cdot 100 \qquad \%\delta Nf\delta\gamma = 55.402 \quad \%$$

$$\%\delta Nf\delta d := \frac{\delta Nf\delta d^2}{\delta Nf^2} \cdot 100 \qquad \%\delta Nf\delta d = 3.523 \quad \%$$

$$\%\delta Nf\delta e := \frac{\delta Nf\delta e^2}{\delta Nf^2} \cdot 100 \qquad \%\delta Nf\delta e = 41.075 \quad \%$$

$$\%\Sigma_{\delta Nf} := \%\delta Nf\delta\gamma + \%\delta Nf\delta d + \%\delta Nf\delta e = 100 \quad \%$$

Cycles to failure Overall Uncertainty: $\delta Nf = 4109.94$

Cycles to failure Percent Overall Uncertainty: $\%\delta Nf = 135.869$ %

Around 5 % uncertainty is deemed acceptable

Min. cycles to failure: $N_f - \delta Nf = -1085.02$ cycles

Min. cycles to failure: $N_f + \delta Nf = 7134.87$ cycles

Experimental :

Thermal Expansion Mismatch Phenomenological Equation: $\tau = \tau(\alpha_s, \alpha_{cc}, T_s, T_{cc}, T_o)$

$$\tau(\alpha_s, \alpha_{cc}, T_s, T_{cc}, T_o) := \alpha_s \cdot (T_s - T_o) - \alpha_{cc} \cdot (T_{cc} - T_o)$$

$$\delta\tau\delta\alpha_s := \frac{\partial}{\partial \alpha_{PCB}} \tau(\alpha_{PCB}, \alpha_{cc}, Tpcb, Tcc, Tamb) \cdot \delta\alpha_s \qquad \delta\tau\delta\alpha_s = 1.26 \times 10^{-5}$$

$$\delta\tau\delta\alpha_{cc} := \frac{\partial}{\partial \alpha_{cc}} \tau(\alpha_{PCB}, \alpha_{cc}, Tpcb, Tcc, Tamb) \cdot \delta\alpha_{cc} \qquad \delta\tau\delta\alpha_{cc} = -4.388 \times 10^{-5}$$

$$\delta\tau\delta T_s := \frac{\partial}{\partial Tpcb} \tau(\alpha_{PCB}, \alpha_{cc}, Tpcb, Tcc, Tamb) \cdot \delta Ts \qquad \delta\tau\delta T_s = 4.95 \times 10^{-5}$$

$$\delta\tau\delta T_{cc} := \frac{\partial}{\partial Tcc} \tau(\alpha_{PCB}, \alpha_{cc}, Tpcb, Tcc, Tamb) \cdot \delta Tcc \qquad \delta\tau\delta T_{cc} = -1.638 \times 10^{-4}$$

$$\delta\tau\delta T_o := \frac{\partial}{\partial Tamb} \tau(\alpha_{PCB}, \alpha_{cc}, Tpcb, Tcc, Tamb) \cdot \delta To \qquad \delta\tau\delta T_o = 8.302 \times 10^{-5}$$

$$\delta\tau e := \left[(\delta\tau\delta\alpha_s)^2 + (\delta\tau\delta\alpha_{cc})^2 + (\delta\tau\delta T_s)^2 + (\delta\tau\delta T_{cc})^2 + (\delta\tau\delta T_o)^2 \right]^{\frac{1}{2}} \qquad \delta\tau e = 1.956 \times 10^{-4}$$

$$\%\delta\tau e := \frac{\delta\tau e}{\tau_{ce}} \cdot 100 \qquad \%\delta\tau = 32.085 \ \%$$

$$\%\delta\tau\delta\alpha_s := \frac{\delta\tau\delta\alpha_s^{\,2}}{\delta\tau e^2} \cdot 100 \qquad \%\delta\tau\delta\alpha_s = 0.415 \ \%$$

$$\%\delta\tau\delta\alpha_{cc} := \frac{\delta\tau\delta\alpha_{cc}^{\,2}}{\delta\tau e^2} \cdot 100 \qquad \%\delta\tau\delta\alpha_{cc} = 5.032 \ \%$$

$$\%\delta\tau\delta T_s := \frac{\delta\tau\delta T_s^{\,2}}{\delta\tau e^2} \cdot 100 \qquad \%\delta\tau\delta T_s = 6.405 \ \%$$

$$\%\delta\tau\delta T_{cc} := \frac{\delta\tau\delta T_{cc}^{\,2}}{\delta\tau e^2} \cdot 100 \qquad \%\delta\tau\delta T_{cc} = 70.131 \ \%$$

$$\%\delta\tau\delta T_o := \frac{\delta\tau\delta T_o^{\,2}}{\delta\tau e^2} \cdot 100 \qquad \%\delta\tau\delta T_o = 18.018 \ \%$$

$$\%\Sigma_{\delta\tau} := \%\delta\tau\delta\alpha_s + \%\delta\tau\delta\alpha_{cc} + \%\delta\tau\delta T_s + \%\delta\tau\delta T_{cc} + \%\delta\tau\delta T_o = 100 \ \%$$

Shear Strain Phenomenological Equation:

$\gamma = \gamma(c, L_o, H, \tau)$

$\gamma(C, L_o, H, \tau) := C \cdot \frac{L_o}{H} \cdot \tau$

$\delta\gamma\delta c := \frac{\partial}{\partial C}\gamma(C, L_o, H, \tau_{ce}) \cdot \delta c$ $\quad \delta\gamma\delta c = 4.253 \times 10^{-3}$

$\delta\gamma\delta L := \frac{\partial}{\partial L_o}\gamma(C, L_o, H, \tau_{ce}) \cdot \delta L$ $\quad \delta\gamma\delta L = 2.296 \times 10^{-3}$

$\delta\gamma\delta H := \frac{\partial}{\partial H}\gamma(C, L_o, H, \tau_{ce}) \cdot \delta H$ $\quad \delta\gamma\delta H = -2.296 \times 10^{-3}$

$\delta\gamma\delta\tau := \frac{\partial}{\partial \tau_{ce}}\gamma(C, L_o, H, \tau_{ce}) \cdot \delta\tau e$ $\quad \delta\gamma\delta\tau = 7.953 \times 10^{-3}$

$\delta\gamma e := \left[(\delta\gamma\delta c)^2 + (\delta\gamma\delta L)^2 + (\delta\gamma\delta H)^2 + (\delta\gamma\delta\tau)^2\right]^{\frac{1}{2}}$ $\quad \delta\gamma e = 9.586 \times 10^{-3}$

$\%\delta\gamma e := \frac{\delta\gamma e}{\gamma_{ce}} \cdot 100$ $\quad \%\delta\gamma e = 41.743$ %

$\%\delta\gamma\delta c := \frac{\delta\gamma\delta c^2}{\delta\gamma e^2} \cdot 100$ $\quad \%\delta\gamma\delta c = 19.681$ %

$\%\delta\gamma\delta L := \frac{\delta\gamma\delta L^2}{\delta\gamma e^2} \cdot 100$ $\quad \%\delta\gamma\delta L = 5.739$ %

$\%\delta\gamma\delta H := \frac{\delta\gamma\delta H^2}{\delta\gamma e^2} \cdot 100$ $\quad \%\delta\gamma\delta H = 5.739$ %

$\%\delta\gamma\delta\tau := \frac{\delta\gamma\delta\tau^2}{\delta\gamma e^2} \cdot 100$ $\quad \%\delta\gamma\delta\tau = 68.841$ %

$\%\Sigma_{\delta\gamma} := \%\delta\gamma\delta c + \%\delta\gamma\delta L + \%\delta\gamma\delta H + \%\delta\gamma\delta\tau$ $\quad \%\Sigma_{\delta\gamma} = 100$ %

Number of Cycles to Failure Phenomenological Equation:

$N_f = Nf(\gamma, d, e)$

$Nf(\gamma, d, e) := \frac{1}{2} \cdot \left(\frac{\gamma}{d}\right)^{\frac{1}{e}}$

$\delta Nf\delta\gamma := \frac{\partial}{\partial \gamma_{ce}} Nf(\gamma_{ce}, d, e) \cdot \delta\gamma e$ $\quad \delta Nf\delta\gamma = -4.19 \times 10^{3}$

$$\delta Nf\delta d := \frac{\partial}{\partial d} Nf(\gamma_{ce}, d, e) \cdot \delta d \qquad \delta Nf\delta d = 1.004 \times 10^{3}$$

$$\delta Nf\delta e := \frac{\partial}{\partial e} Nf(\gamma_{ce}, d, e) \cdot \delta e \qquad \delta Nf\delta e = -3.53 \times 10^{3}$$

$$\delta Nfe := \left[(\delta Nf\delta\gamma)^2 + (\delta Nf\delta d)^2 + (\delta Nf\delta e)^2 \right]^{\frac{1}{2}} \qquad \delta Nfe = 5.57 \times 10^{3}$$

$$\%\delta Nfe := \frac{\delta Nfe}{N_{fe}} \cdot 100 \qquad \%\delta Nfe = 141.534 \quad \%$$

$$\%\delta Nf\delta\gamma := \frac{\delta Nf\delta\gamma^2}{\delta Nfe^2} \cdot 100 \qquad \%\delta Nf\delta\gamma = 56.578 \quad \%$$

$$\%\delta Nf\delta d := \frac{\delta Nf\delta d^2}{\delta Nfe^2} \cdot 100 \qquad \%\delta Nf\delta d = 3.247 \quad \%$$

$$\%\delta Nf\delta e := \frac{\delta Nf\delta e^2}{\delta Nfe^2} \cdot 100 \qquad \%\delta Nf\delta e = 40.175 \quad \%$$

$$\%\Sigma_{\delta Nf} := \%\delta Nf\delta\gamma + \%\delta Nf\delta d + \%\delta Nf\delta e = 100 \quad \%$$

Cycles to failure Overall Uncertainty: $\delta Nfe = 5569.94$

Cycles to failure Percent Overall Uncertainty: $\%\delta Nfe = 141.53$ %

Around 5 % uncertainty is deemed acceptable

Min. cycles to failure: $N_{fe} - \delta Nfe = -1634.52$ cycles

Min. cycles to failure: $N_{fe} + \delta Nfe = 9505.36$ cycles

Trial#2 Uncertainty Analysis:

Uncertainties:

$\delta\alpha_{PCB} := 1\% \cdot \alpha_{PCB} = 1.8 \times 10^{-7}$ 1/K

$\delta\alpha_{cc} := 1\% \cdot \alpha_{cc} = 5.85 \times 10^{-7}$ 1/K

$\delta L := 1\% \cdot L_o = 0.032$ mm

$\delta H := 1\% \cdot H = 1.05 \times 10^{-3}$ mm

$\delta d := 0.00005$

$\delta e := 0.00005$

$\delta c := 0.005$

Comsol values:			*Experimental values:*	
$\delta T_{amb} := (T_{amb} - 273.15) \cdot 0.5\% = 0.1$	K		$\delta To := (Tamb) \cdot 0.5\% = 0.103$	°C
$\delta T_{PCB} := (T_{PCB} - 273.15) \cdot 1\% = 0.255$	K		$\delta Ts := (Tpcb) \cdot 1\% = 0.275$	°C
$\delta T_{cc} := (T_{cc} - 273.15) \cdot 0.1\% = 0.029$	K		$\delta Tcc := (Tcc) \cdot 0.1\% = 0.028$	°C

For Comsol Values:

Thermal Expansion Mismatch Phenomenological Equation:

$$\tau = \tau(\alpha_s, \alpha_{cc}, T_s, T_{cc}, T_o)$$

$$\tau(\alpha_s, \alpha_{cc}, T_s, T_{cc}, T_o) := \alpha_s \cdot (T_s - T_o) - \alpha_{cc} \cdot (T_{cc} - T_o)$$

$$\delta\tau\delta\alpha_s := \frac{\partial}{\partial \alpha_{PCB}} \tau(\alpha_{PCB}, \alpha_{cc}, T_{PCB}, T_{cc}, T_{amb}) \cdot \delta\alpha_s \qquad \delta\tau\delta\alpha_s = 9.865 \times 10^{-7}$$

$$\delta\tau\delta\alpha_{cc} := \frac{\partial}{\partial \alpha_{cc}} \tau(\alpha_{PCB}, \alpha_{cc}, T_{PCB}, T_{cc}, T_{amb}) \cdot \delta\alpha_{cc} \qquad \delta\tau\delta\alpha_{cc} = -5.275 \times 10^{-6}$$

$$\delta\tau\delta T_s := \frac{\partial}{\partial T_{PCB}} \tau(\alpha_{PCB}, \alpha_{cc}, T_{PCB}, T_{cc}, T_{amb}) \cdot \delta T_s \qquad \delta\tau\delta T_s = 4.587 \times 10^{-6}$$

$$\delta\tau\delta T_{cc} := \frac{\partial}{\partial T_{cc}} \tau(\alpha_{PCB}, \alpha_{cc}, T_{PCB}, T_{cc}, T_{amb}) \cdot \delta T_{cc} \qquad \delta\tau\delta T_{cc} = -1.697 \times 10^{-6}$$

$$\delta\tau\delta T_o := \frac{\partial}{\partial T_{amb}} \tau(\alpha_{PCB}, \alpha_{cc}, T_{PCB}, T_{cc}, T_{amb}) \cdot \delta T_o \qquad \delta\tau\delta T_o = 4.05 \times 10^{-6}$$

$$\delta\tau := \left[(\delta\tau\delta\alpha_s)^2 + (\delta\tau\delta\alpha_{cc})^2 + (\delta\tau\delta T_s)^2 + (\delta\tau\delta T_{cc})^2 + (\delta\tau\delta T_o)^2 \right]^{\frac{1}{2}} \qquad \delta\tau = 8.314 \times 10^{-6}$$

$$\%\delta\tau := \frac{\delta\tau}{\tau_c} \cdot 100 \qquad \%\delta\tau = 1.328 \ \%$$

$$\%\delta\tau\delta\alpha_s := \frac{\delta\tau\delta\alpha_s^{\,2}}{\delta\tau^2} \cdot 100 \qquad \%\delta\tau\delta\alpha_s = 1.408 \ \%$$

$$\%\delta\tau\delta\alpha_{cc} := \frac{\delta\tau\delta\alpha_{cc}^{\,2}}{\delta\tau^2} \cdot 100 \qquad \%\delta\tau\delta\alpha_{cc} = 40.255 \ \%$$

$$\%\delta\tau\delta T_s := \frac{\delta\tau\delta T_s^{\,2}}{\delta\tau^2} \cdot 100 \qquad \%\delta\tau\delta T_s = 30.436 \ \%$$

$$\%\delta\tau\delta T_{cc} := \frac{\delta\tau\delta T_{cc}^{\,2}}{\delta\tau^2} \cdot 100 \qquad \%\delta\tau\delta T_{cc} = 4.169 \ \%$$

$$\%\delta\tau\delta T_o := \frac{\delta\tau\delta T_o^{\,2}}{\delta\tau^2} \cdot 100 \qquad \%\delta\tau\delta T_o = 23.732 \ \%$$

$$\%\Sigma_{\delta\tau} := \%\delta\tau\delta\alpha_s + \%\delta\tau\delta\alpha_{cc} + \%\delta\tau\delta T_s + \%\delta\tau\delta T_{cc} + \%\delta\tau\delta T_o = 100 \ \%$$

Shear Strain Phenomenological Equation: $\gamma = \gamma(c, L_o, H, \tau)$

$$\gamma(C, L_o, H, \tau) := C \cdot \frac{L_o}{H} \cdot \tau$$

$$\delta\gamma\delta c := \frac{\partial}{\partial C}\gamma(C, L_o, H, \tau_c) \cdot \delta c \qquad \delta\gamma\delta c = 9.43 \times 10^{-5}$$

$$\delta\gamma\delta L := \frac{\partial}{\partial L_o}\gamma(C, L_o, H, \tau_c) \cdot \delta L \qquad \delta\gamma\delta L = 2.546 \times 10^{-4}$$

$$\delta\gamma\delta H := \frac{\partial}{\partial H}\gamma(C, L_o, H, \tau_c) \cdot \delta H \qquad \delta\gamma\delta H = -2.546 \times 10^{-4}$$

$$\delta\gamma\delta\tau := \frac{\partial}{\partial \tau_c}\gamma(C, L_o, H, \tau_c) \cdot \delta\tau \qquad \delta\gamma\delta\tau = 3.381 \times 10^{-4}$$

$$\delta\gamma := \left[(\delta\gamma\delta c)^2 + (\delta\gamma\delta L)^2 + (\delta\gamma\delta H)^2 + (\delta\gamma\delta\tau)^2\right]^{\frac{1}{2}} \qquad \delta\gamma = 5.028 \times 10^{-4}$$

$$\%\delta\gamma := \frac{\delta\gamma}{\gamma_c} \cdot 100 \qquad \%\delta\gamma = 1.975 \ \%$$

$$\%\delta\gamma\delta c := \frac{\delta\gamma\delta c^2}{\delta\gamma^2} \cdot 100 \qquad \%\delta\gamma\delta c = 3.517 \ \%$$

$$\%\delta\gamma\delta L := \frac{\delta\gamma\delta L^2}{\delta\gamma^2} \cdot 100 \qquad \%\delta\gamma\delta L = 25.64 \ \%$$

$$\%\delta\gamma\delta H := \frac{\delta\gamma\delta H^2}{\delta\gamma^2} \cdot 100 \qquad \%\delta\gamma\delta H = 25.64 \ \%$$

$$\%\delta\gamma\delta\tau := \frac{\delta\gamma\delta\tau^2}{\delta\gamma^2} \cdot 100 \qquad \%\delta\gamma\delta\tau = 45.203 \ \%$$

$$\%\Sigma_{\delta\gamma} := \%\delta\gamma\delta c + \%\delta\gamma\delta L + \%\delta\gamma\delta H + \%\delta\gamma\delta\tau \qquad \%\Sigma_{\delta\gamma} = 100 \ \%$$

Number of Cycles to Failure Phenomenological Equation: $N_f = Nf(\gamma, d, e)$

$$Nf(\gamma, d, e) := \frac{1}{2} \cdot \left(\frac{\gamma}{d}\right)^{\frac{1}{e}}$$

$$\delta Nf\delta\gamma := \frac{\partial}{\partial \gamma_c} Nf(\gamma_c, d, e) \cdot \delta\gamma \qquad \delta Nf\delta\gamma = -152.356$$

$$\delta Nf\delta d := \frac{\partial}{\partial d} Nf(\gamma_c, d, e) \cdot \delta d \qquad \delta Nf\delta d = 0.498$$

$$\delta Nf\delta e := \frac{\partial}{\partial e} Nf(\gamma_c, d, e) \cdot \delta e \qquad \delta Nf\delta e = 3.359$$

$$\delta Nf := \left[(\delta Nf\delta\gamma)^2 + (\delta Nf\delta d)^2 + (\delta Nf\delta e)^2 \right]^{\frac{1}{2}} \qquad \delta Nf = 152.394$$

$$\%\delta Nf := \frac{\delta Nf}{N_f} \cdot 100 \qquad \%\delta Nf = 5.038 \ \%$$

$$\%\delta Nf\delta\gamma := \frac{\delta Nf\delta\gamma^2}{\delta Nf^2} \cdot 100 \qquad \%\delta Nf\delta\gamma = 99.95 \ \%$$

$$\%\delta Nf\delta d := \frac{\delta Nf\delta d^2}{\delta Nf^2} \cdot 100 \qquad \%\delta Nf\delta d = 1.07 \times 10^{-3} \ \%$$

$$\%\delta Nf\delta e := \frac{\delta Nf\delta e^2}{\delta Nf^2} \cdot 100 \qquad \%\delta Nf\delta e = 0.049 \ \%$$

$$\%\Sigma_{\delta Nf} := \%\delta Nf\delta\gamma + \%\delta Nf\delta d + \%\delta Nf\delta e = 100 \ \%$$

Cycles to failure Overall Uncertainty: $\delta Nf = 152.39$

Cycles to failure Percent Overall Uncertainty: $\%\delta Nf = 5.038$ %

Around 5 % uncertainty is deemed acceptable

Min. cycles to failure: $N_f - \delta Nf = 2872.53$ cycles

Min. cycles to failure: $N_f + \delta Nf = 3177.32$ cycles

Experimental :

Thermal Expansion Mismatch Phenomenological Equation: $\tau = \tau(\alpha_s, \alpha_{cc}, T_s, T_{cc}, T_o)$

$$\tau(\alpha_s, \alpha_{cc}, T_s, T_{cc}, T_o) := \alpha_s \cdot (T_s - T_o) - \alpha_{cc} \cdot (T_{cc} - T_o)$$

$$\delta\tau\delta\alpha_s := \frac{\partial}{\partial \alpha_{PCB}} \tau(\alpha_{PCB}, \alpha_{cc}, Tpcb, Tcc, Tamb) \cdot \delta\alpha_s \qquad \delta\tau\delta\alpha_s = 1.26 \times 10^{-6}$$

$$\delta\tau\delta\alpha_{cc} := \frac{\partial}{\partial \alpha_{cc}} \tau(\alpha_{PCB}, \alpha_{cc}, Tpcb, Tcc, Tamb) \cdot \delta\alpha_{cc} \qquad \delta\tau\delta\alpha_{cc} = -4.388 \times 10^{-6}$$

$$\delta\tau\delta T_s := \frac{\partial}{\partial Tpcb} \tau(\alpha_{PCB}, \alpha_{cc}, Tpcb, Tcc, Tamb) \cdot \delta Ts \qquad \delta\tau\delta T_s = 4.95 \times 10^{-6}$$

$$\delta\tau\delta T_{cc} := \frac{\partial}{\partial Tcc} \tau(\alpha_{PCB}, \alpha_{cc}, Tpcb, Tcc, Tamb) \cdot \delta Tcc \qquad \delta\tau\delta T_{cc} = -1.638 \times 10^{-6}$$

$$\delta\tau\delta T_o := \frac{\partial}{\partial Tamb} \tau(\alpha_{PCB}, \alpha_{cc}, Tpcb, Tcc, Tamb) \cdot \delta To \qquad \delta\tau\delta T_o = 4.151 \times 10^{-6}$$

$$\delta\tau e := \left[(\delta\tau\delta\alpha_s)^2 + (\delta\tau\delta\alpha_{cc})^2 + (\delta\tau\delta T_s)^2 + (\delta\tau\delta T_{cc})^2 + (\delta\tau\delta T_o)^2 \right]^{\frac{1}{2}} \qquad \delta\tau e = 8.078 \times 10^{-6}$$

$$\%\delta\tau e := \frac{\delta\tau e}{\tau_{ce}} \cdot 100 \qquad \%\delta\tau = 1.328 \ \%$$

$$\%\delta\tau\delta\alpha_s := \frac{\delta\tau\delta\alpha_s^{\,2}}{\delta\tau e^2} \cdot 100 \qquad \%\delta\tau\delta\alpha_s = 2.433 \ \%$$

$$\%\delta\tau\delta\alpha_{cc} := \frac{\delta\tau\delta\alpha_{cc}^{\,2}}{\delta\tau e^2} \cdot 100 \qquad \%\delta\tau\delta\alpha_{cc} = 29.499 \ \%$$

$$\%\delta\tau\delta T_s := \frac{\delta\tau\delta T_s^{\,2}}{\delta\tau e^2} \cdot 100 \qquad \%\delta\tau\delta T_s = 37.548 \ \%$$

$$\%\delta\tau\delta T_{cc} := \frac{\delta\tau\delta T_{cc}^{\,2}}{\delta\tau e^2} \cdot 100 \qquad \%\delta\tau\delta T_{cc} = 4.112 \ \%$$

$$\%\delta\tau\delta T_o := \frac{\delta\tau\delta T_o^{\,2}}{\delta\tau e^2} \cdot 100 \qquad \%\delta\tau\delta T_o = 26.408 \ \%$$

$$\%\Sigma_{\delta\tau} := \%\delta\tau\delta\alpha_s + \%\delta\tau\delta\alpha_{cc} + \%\delta\tau\delta T_s + \%\delta\tau\delta T_{cc} + \%\delta\tau\delta T_o = 100 \ \%$$

Shear Strain Phenomenological Equation:

$\gamma = \gamma(c, L_o, H, \tau)$

$\gamma(C, L_o, H, \tau) := C \cdot \frac{L_o}{H} \cdot \tau$

$\delta\gamma\delta c := \frac{\partial}{\partial C}\gamma(C, L_o, H, \tau_{ce}) \cdot \delta c$ $\quad \delta\gamma\delta c = 8.505 \times 10^{-5}$

$\delta\gamma\delta L := \frac{\partial}{\partial L_o}\gamma(C, L_o, H, \tau_{ce}) \cdot \delta L$ $\quad \delta\gamma\delta L = 2.296 \times 10^{-4}$

$\delta\gamma\delta H := \frac{\partial}{\partial H}\gamma(C, L_o, H, \tau_{ce}) \cdot \delta H$ $\quad \delta\gamma\delta H = -2.296 \times 10^{-4}$

$\delta\gamma\delta\tau := \frac{\partial}{\partial \tau_{ce}}\gamma(C, L_o, H, \tau_{ce}) \cdot \delta\tau e$ $\quad \delta\gamma\delta\tau = 3.285 \times 10^{-4}$

$\delta\gamma e := \left[(\delta\gamma\delta c)^2 + (\delta\gamma\delta L)^2 + (\delta\gamma\delta H)^2 + (\delta\gamma\delta\tau)^2\right]^{\frac{1}{2}}$ $\quad \delta\gamma e = 4.697 \times 10^{-4}$

$\%\delta\gamma e := \frac{\delta\gamma e}{\gamma_{ce}} \cdot 100$ $\quad \%\delta\gamma e = 2.045$ %

$\%\delta\gamma\delta c := \frac{\delta\gamma\delta c^2}{\delta\gamma e^2} \cdot 100$ $\quad \%\delta\gamma\delta c = 3.279$ %

$\%\delta\gamma\delta L := \frac{\delta\gamma\delta L^2}{\delta\gamma e^2} \cdot 100$ $\quad \%\delta\gamma\delta L = 23.905$ %

$\%\delta\gamma\delta H := \frac{\delta\gamma\delta H^2}{\delta\gamma e^2} \cdot 100$ $\quad \%\delta\gamma\delta H = 23.905$ %

$\%\delta\gamma\delta\tau := \frac{\delta\gamma\delta\tau^2}{\delta\gamma e^2} \cdot 100$ $\quad \%\delta\gamma\delta\tau = 48.91$ %

$\%\Sigma_{\delta\gamma} := \%\delta\gamma\delta c + \%\delta\gamma\delta L + \%\delta\gamma\delta H + \%\delta\gamma\delta\tau$ $\quad \%\Sigma_{\delta\gamma} = 100$ %

Number of Cycles to Failure Phenomenological Equation:

$N_f = Nf(\gamma, d, e)$

$Nf(\gamma, d, e) := \frac{1}{2} \cdot \left(\frac{\gamma}{d}\right)^{\frac{1}{e}}$

$\delta Nf\delta\gamma := \frac{\partial}{\partial \gamma_{ce}} Nf(\gamma_{ce}, d, e) \cdot \delta\gamma e$ $\quad \delta Nf\delta\gamma = -205.281$

$$\delta Nf\delta d := \frac{\partial}{\partial d} Nf\left(\gamma_{ce}, d, e\right) \cdot \delta d \qquad \delta Nf\delta d = 0.648$$

$$\delta Nf\delta e := \frac{\partial}{\partial e} Nf\left(\gamma_{ce}, d, e\right) \cdot \delta e \qquad \delta Nf\delta e = 4.502$$

$$\delta Nfe := \left[(\delta Nf\delta\gamma)^2 + (\delta Nf\delta d)^2 + (\delta Nf\delta e)^2\right]^{\frac{1}{2}} \qquad \delta Nfe = 205.331$$

$$\%\delta Nfe := \frac{\delta Nfe}{N_{fe}} \cdot 100 \qquad \%\delta Nfe = 5.218 \ \%$$

$$\%\delta Nf\delta\gamma := \frac{\delta Nf\delta\gamma^2}{\delta Nfe^2} \cdot 100 \qquad \%\delta Nf\delta\gamma = 99.951 \ \%$$

$$\%\delta Nf\delta d := \frac{\delta Nf\delta d^2}{\delta Nfe^2} \cdot 100 \qquad \%\delta Nf\delta d = 9.974 \times 10^{-4} \ \%$$

$$\%\delta Nf\delta e := \frac{\delta Nf\delta e^2}{\delta Nfe^2} \cdot 100 \qquad \%\delta Nf\delta e = 0.048 \ \%$$

$$\%\Sigma_{\delta Nfe} := \%\delta Nf\delta\gamma + \%\delta Nf\delta d + \%\delta Nf\delta e = 100 \ \%$$

Cycles to failure Overall Uncertainty: $\delta Nfe = 205.33$

Cycles to failure Percent Overall Uncertainty: $\%\delta Nfe = 5.22$ %

Around 5 % uncertainty is deemed acceptable

Min. cycles to failure: $N_{fe} - \delta Nfe = 3730.09$ cycles

Min. cycles to failure: $N_{fe} + \delta Nfe = 4140.75$ cycles

Transient Analysis:

$T_{sol} :=$

	0
0	293.343
1	...

$Ts(t) := T_{sol_t}$ $t := 0, 10 .. 720$

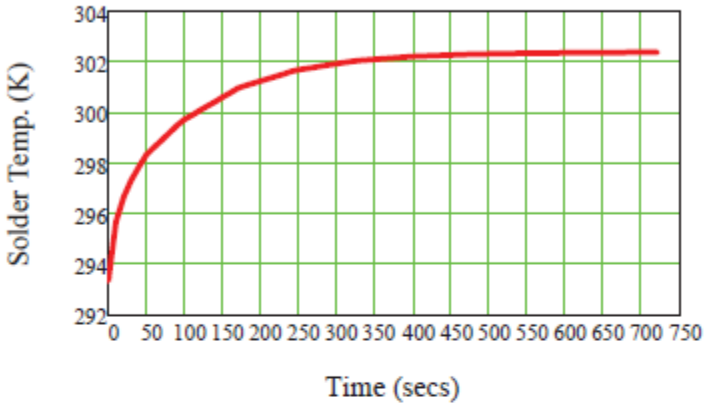

$\sigma_{svM} :=$

	0
0	0.034
1	...

$\varepsilon Ts :=$

	0
0	$4.051 \cdot 10^{-6}$
1	...

$\sigma svM(t) := \sigma_{svM_t}$ MPa

$\varepsilon Ts(t) := \varepsilon Ts_t$

Uncertainties:

$\delta\alpha S := \alpha_S \cdot 2.5\% = 5.25 \times 10^{-7}$ 1/K

$\delta TS := (T_S - 273.15) \cdot 2.5\% = 0.731$ K

$\delta ES := E_S \cdot 5\% = 500$ MPa

Thermal strain phenomenological equation: $\varepsilon = \varepsilon(\alpha_S, T_S, T_{amb})$

$\varepsilon(\alpha, T1, T2) := \alpha \cdot (T1 - T2)$

$\varepsilon tts := \varepsilon(\alpha_S, T_S, T_{amb}) = 1.937 \times 10^{-4}$

$\delta\varepsilon\delta\alpha S := \frac{d}{d\alpha_S}\varepsilon(\alpha_S, T_S, T_{amb}) \cdot \delta\alpha S$ $\delta\varepsilon\delta\alpha S = 4.843 \times 10^{-6}$

$\delta\varepsilon\delta TS := \frac{d}{dT_S}\varepsilon(\alpha_S, T_S, T_{amb}) \cdot \delta TS$ $\delta\varepsilon\delta TS = 1.534 \times 10^{-5}$

$$\delta\epsilon\delta Ta := \frac{d}{dT_{amb}}\epsilon\left(\alpha_S, T_S, T_{amb}\right)\cdot\delta T_o \qquad \delta\epsilon\delta\alpha S = 4.843\times10^{-6}$$

$$\delta\epsilon := \sqrt{\delta\epsilon\delta\alpha S^2 + \delta\epsilon\delta TS^2 + \delta\epsilon\delta Ta^2} \qquad \delta\epsilon = 1.623\times10^{-5}$$

$$\%\delta\epsilon := \frac{\delta\epsilon}{\epsilon\left(\alpha_S, T_S, T_{amb}\right)}\cdot100 \qquad \%\delta\epsilon = 8.376$$

Thermal strain phenomenological equation: $\sigma = \sigma(E, \epsilon)$

$$\sigma tS(E, \epsilon ts) := E\cdot\epsilon ts$$

$$\sigma tts := \sigma tS\left(E_S, \epsilon tts\right) = 1.937$$

$$\delta\sigma\delta E := \frac{d}{dE_S}\sigma tS\left(E_S, \epsilon tts\right)\cdot\delta ES \qquad \delta\sigma\delta E = 0.097$$

$$\delta\sigma\delta\epsilon := \frac{d}{d\epsilon tts}\sigma tS\left(E_S, \epsilon tts\right)\cdot\delta\epsilon \qquad \delta\sigma\delta\epsilon = 0.162$$

$$\delta\sigma := \sqrt{\delta\sigma\delta E^2 + \delta\sigma\delta\epsilon^2} \qquad \delta\sigma = 0.189$$

$$\%\delta\sigma := \frac{\delta\sigma}{\sigma tts}\cdot100 \qquad \%\delta\sigma = 9.755$$

Analysis :

$$\epsilon TS(t) := \alpha_S\cdot\left(Ts(t) - T_{amb}\right)$$

$$\sigma TS(t) := E_S\cdot\epsilon TS(t)$$

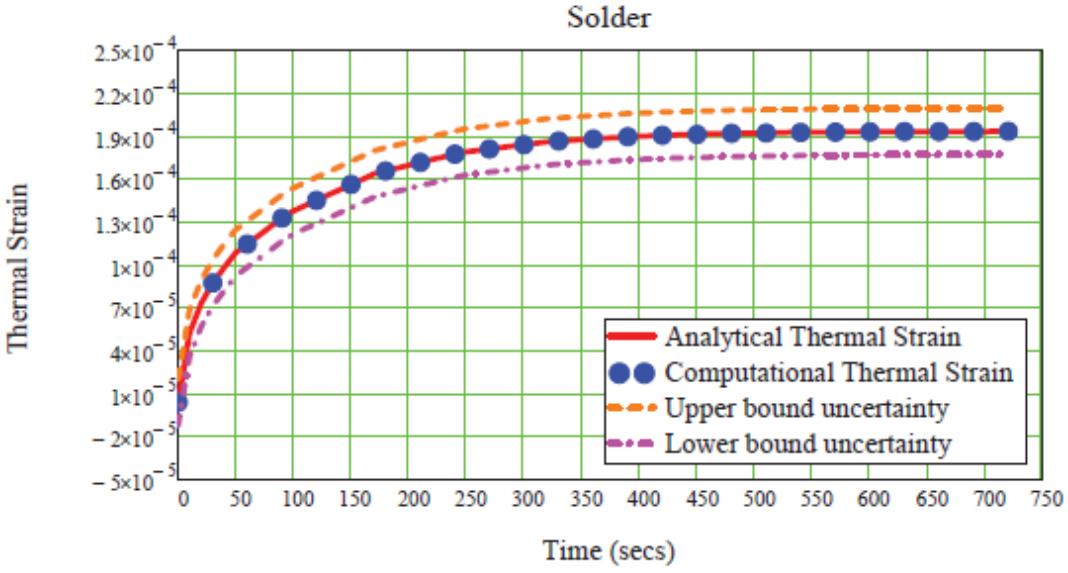

Lin-Log representation:

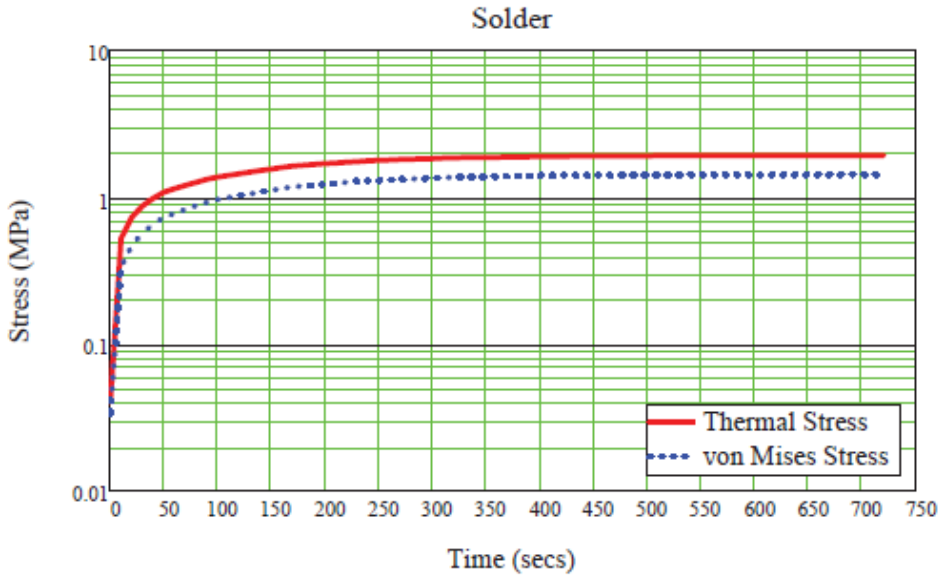

Linn-Lin representation

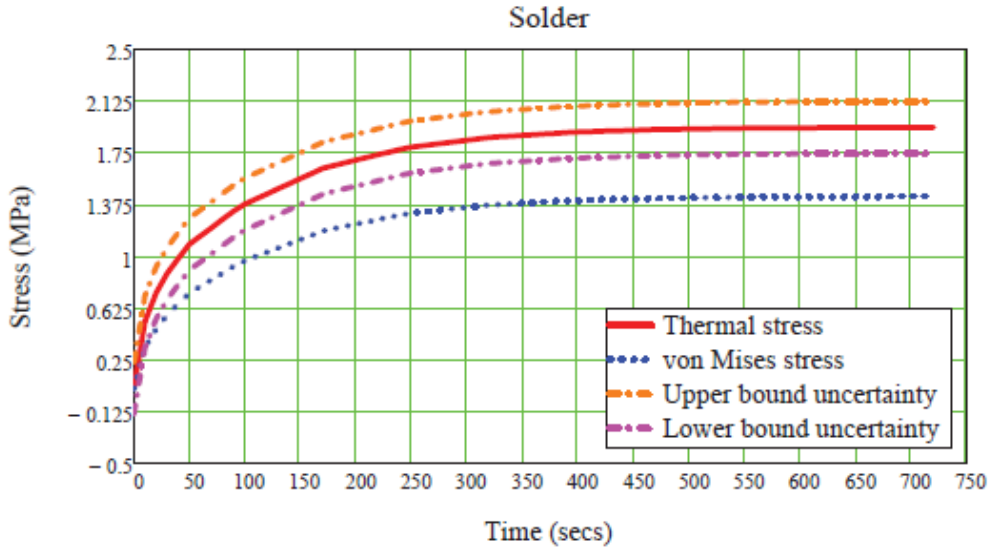

$$FS1(t) := \frac{\sigma_{yS}}{\sigma TS(t)} \qquad FS2(t) := \frac{\sigma_{yS}}{\sigma svM(t)}$$

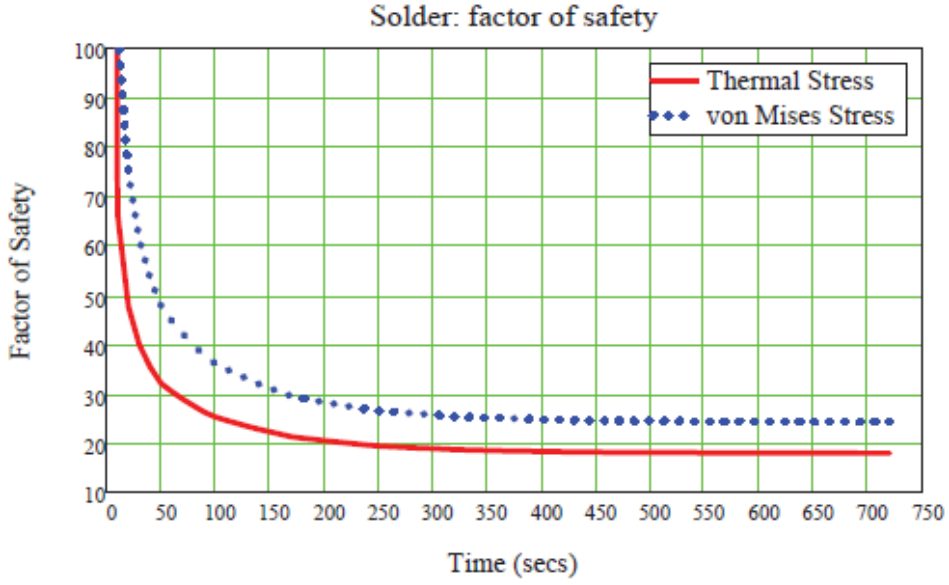

TPCB :=

	0
0	293.152
1	...

Tcc :=

	0
0	293.183
1	...

$Tpcb(t) := TPCB_t$

$TCC(t) := Tcc_t$

$\tau c(t) := \alpha_{PCB} \cdot (Tpcb(t) - T_{amb}) + \alpha_{cc} \cdot (TCC(t) - T_{amb})$

$\gamma c(t) := C \cdot \frac{L_o}{H} \cdot \tau c(t)$

$\sigma\tau(t) := E_S \cdot \tau c(t)$

$\sigma\gamma(t) := E_S \cdot \gamma c(t)$

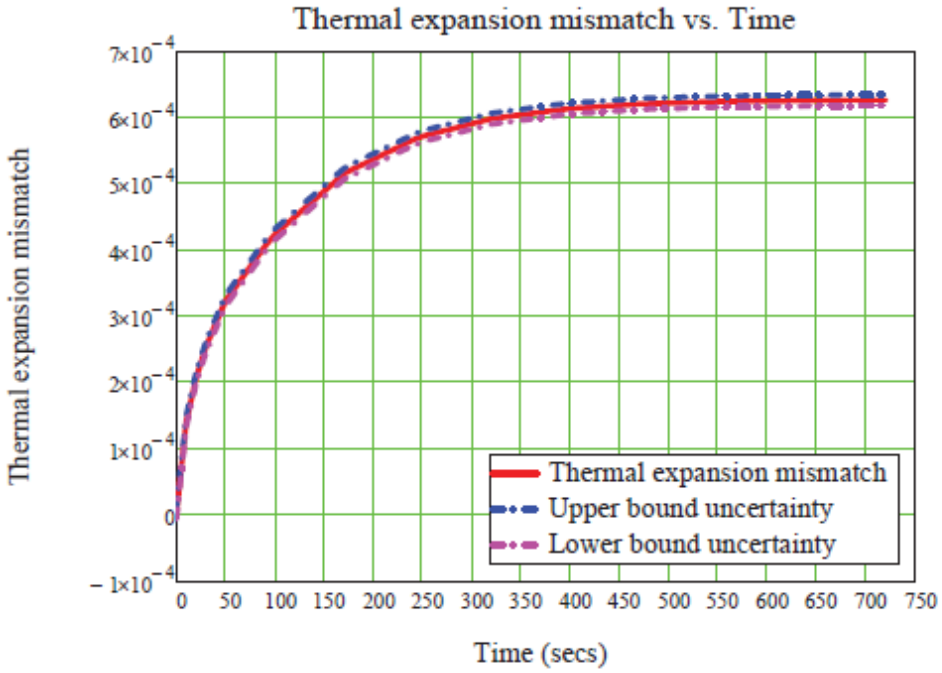
Thermal expansion mismatch vs. Time
Thermal expansion mismatch
Time (secs)
Thermal expansion mismatch
Upper bound uncertainty
Lower bound uncertainty

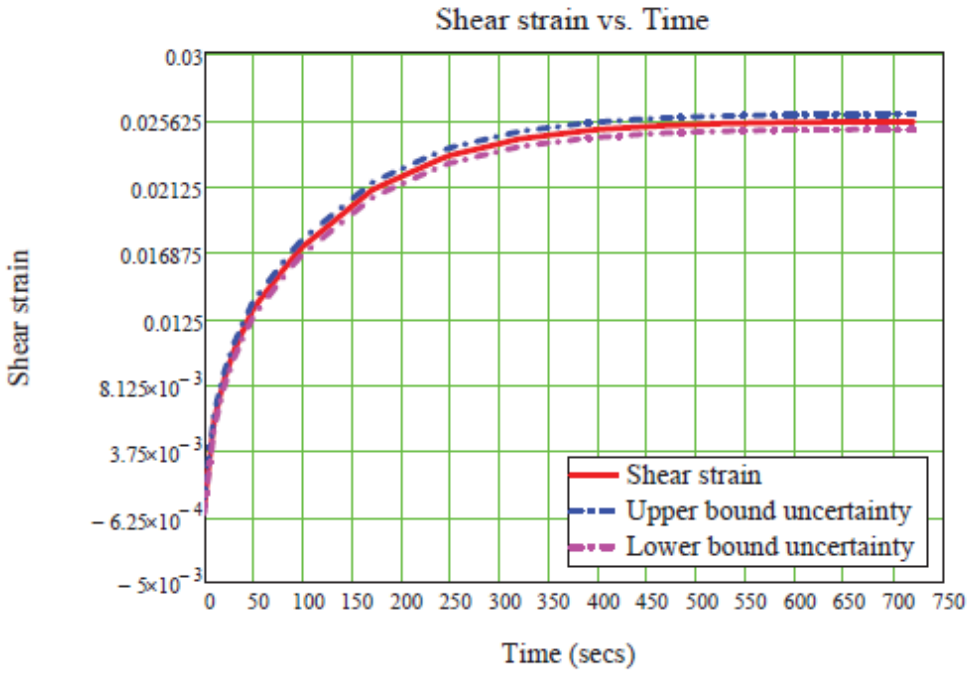
Shear strain vs. Time
Shear strain
Time (secs)
Shear strain
Upper bound uncertainty
Lower bound uncertainty

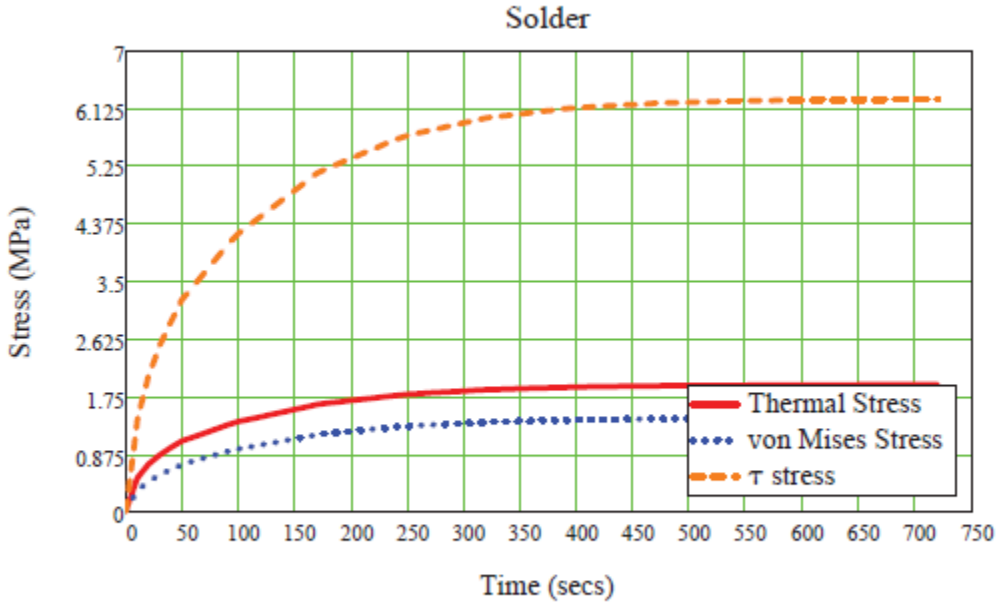
Solder
Stress (MPa)
7
6.125
5.25
4.375
3.5
2.625
1.75
0.875
0
0
50
100
150
200
250
300
350
400
450
500
550
600
650
700
750
Time (secs)
Thermal Stress
von Mises Stress
τ stress

Analysis of the Thermo-Mechanical Reliability of an SMT Attachment

Authors: Roberto Alvarado, Michael Bartlett, Richard Beski, Santiago Isaza, Congji Li
Advisor: Professor Ryszard J. Pryputniewicz Co-Advisor: Professor Germano Iannacchione
Mechanical Engineering Department & Physics Department
2013

Objective

The objective of this project was to analyze the reliability of surface mounted technology (SMT) attachments which are subjected to electrical, thermal, and mechanical loads. Since microsystems, microelectronics, and microelectromechanical systems (MEMS) are being increasingly integrated into society and everyday life, their reliability is of major concern. Of the many factors contributing to SMT reliability, this project aims to identify the most prevalent issues through modeling and uncertainty analysis.

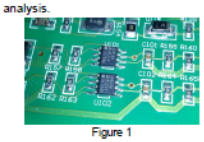

Figure 1

SMT is defined as a methodology for attaching packages directly to the surface of a printed circuit board (PCB) by way of a solder joint. This methodology increases component density by allowing components to be attached on both sides of the PCB.

Issues plaguing SMTs

1. **Thermal cycling issues:** These are issues that are brought about by the cycling process of heating and reheating of components due to certain conditions and loads experienced under normal usage (Ghaffarian 1995).
2. **Power cycling issues:** Power cycling is in essence the continuous cycling between the on and off states of a component or set of components. This is useful because it acts as a simulator for the operational performance or the cycles to failure of the tested components.
3. **Vibrational issues:** This is the issue that SMTs suffer when subjected to an environment that causes vibrations, whether it be the shock from a fall or the shaking of components due to other external factors such as the movement of machinery or transportation and shipping (Blattau, 2012).
4. **Material property issues:** These issues focus on the material properties of the solder used to attach components. Material analysis allows us to study the intermetallic compounds and bonds within the solder that gives the solder its strength (Tu, et al. 1997).

The ACES methodology

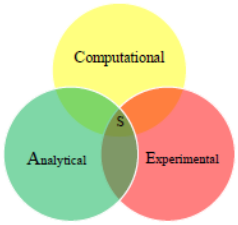

Pioneered by our advisor, the ACES methodology is a solutions approach to analyzing problems through Analytical, Computational and Experimental methods. By addressing each of these methods we gain a more wholesome understanding of the issue at hand, as well as mutual confirmation for each of the methods employed.

Analytical: MathCad calculations

$$T_{em} := \frac{1}{4}\left(3\,T_{amb} + T_{PCB} + T_{ct}\right) \qquad T_c := \alpha_{PCB}\left(T_{PCB} - T_{amb}\right) + \alpha_{ct}\left(T_{ct} - T_{amb}\right)$$

$$\gamma_c = C\frac{\tau_o}{H}\,\tau_t \qquad H_F = \left(\frac{1}{2}\right)\left(\frac{\gamma_c}{\sigma}\right)^{\left(\frac{1}{n}\right)}$$

Using MathCad we were able to determine the temperature uncertainty for each of the package's components.

Computational: modeling and finite element analysis

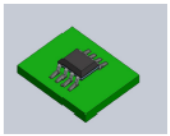

Figure 2

Figure 3

Using SolidWorks, our group was able to model AD623A, a single supply amplifier, using the specifications listed in the chip's data sheet (Analog Devices, 2008). We were then able to import our model into COMSOL Multiphysics for simulation testing. We found that since the model was symmetric, we only needed a quarter model which allowed for shortened calculation times.

Experimental

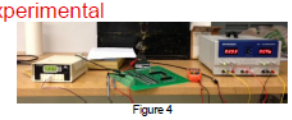

Figure 4

Figure 5

To test the thermal response of AD623A, we used a single thermocouple to measure the temperature distribution throughout the package. Comparison of the experimental data with the analytical and computational results demonstrated correlation within uncertainty limits.

Results and discussion

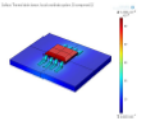

Figure 6

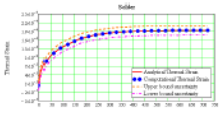

Figure 7

$$\epsilon_{TS} = \alpha_S\left(T_S - T_{amb}\right)$$

Through our computational model, we were able to easily recognize that the thermal strain was more heavily concentrated on the chip carrier than on any other part of the system, peaking at roughly 4 x 10^{-4}. The solder used to connect the component to the PCB exhibits the second largest amount of thermal strain of about 2 x 10^{-4}.

Results and discussion

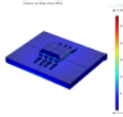

Figure 8

$$\sigma_{TS} = S_E\,\epsilon_{TS}$$

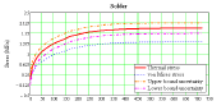

Figure 9

Both figures 8 and 9 indicate a relatively low overall stress within the component and the system. The level of stress present within the solder, as shown by figure 9, levels out at nearly 2 MPa after about 550 seconds.

Figure 10

$$FS = \frac{\sigma_{all}}{\sigma_{max}}$$

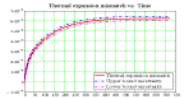

Figure 11

Despite the curve presented in figure 10, the factor of safety determined for this component was found to be around 20. Under the given conditions, the thermal expansion mismatch (depicted in figure 11) begins to level off at nearly 6 x 10^{-4} K^{-1} at a time of 500 seconds.

Conclusion

Through the comparison of the computational modeling and analytical (graphical) results, we were able to show consistent findings across the different solution methods. Both the analytical and computational values were shown to fall within the limits of the measured uncertainty values. For each measured value we observed a monotonic progression, indicating the absence of fluctuation in these values over time. The correlation between the results of the different solution methods validates the ability to accurately model components and the conditions that they experience in functional applications.

Reflection

After completing the project, the group discussed the technical issues that we faced and what we would have done if given the opportunity to redo the project. One of the biggest lessons we learned was to not invest too much time on potential contacts. With all the time spent, we could have focused more time on computational and analytical analysis.

References

- Analog Devices. (2008). AD623 Chip.
- Blattau, D. N. (2012, February 23). Exploring Vibration Fatigue of Electronic Assemblies. College Park, Maryland.
- Ghaffarian, D. R. (1995). SMT Solder Joint Reliability/Workmanship Environmental Test Results Correlation for LCC Assemblies. Pasadena, California.
- Tu, P. L., Chan, Y. C., Lai, J. K. (1997, February). Effect of Intermetallic Compounds on the Thermal Fatigue of Surface Mount Solder Joints. *IEEE Transactions on Components, Packaging, and Manufacturing Technology, 20*(1), pp. 87-93.